5-2014

A Bayesian Approach to Broad-Area Nuclear and Radiological Search Operations

Samuel James Willmon
University of Tennessee - Knoxville, swillmon@utk.edu

To the Graduate Council:

I am submitting herewith a dissertation written by Samuel James Willmon entitled "A Bayesian Approach to Broad-Area Nuclear and Radiological Search Operations." I have examined the final electronic copy of this dissertation for form and content and recommend that it be accepted in partial fulfillment of the requirements for the degree of Doctor of Philosophy, with a major in Nuclear Engineering.

Howard L. Hall, Major Professor

We have read this dissertation and recommend its acceptance:

Ronald E. Pevey, Jason P. Hayward, Glenn O. Allgood

Accepted for the Council:
Dixie L. Thompson

Vice Provost and Dean of the Graduate School

(Original signatures are on file with official student records.)

5-2014

A Bayesian Approach to Broad-Area Nuclear and Radiological Search Operations

Samuel James Willmon
University of Tennessee - Knoxville, swillmon@utk.edu

To the Graduate Council:

I am submitting herewith a dissertation written by Samuel James Willmon entitled "A Bayesian Approach to Broad-Area Nuclear and Radiological Search Operations." I have examined the final electronic copy of this dissertation for form and content and recommend that it be accepted in partial fulfillment of the requirements for the degree of Doctor of Philosophy, with a major in Nuclear Engineering.

Howard L. Hall, Major Professor

We have read this dissertation and recommend its acceptance:

Ronald E. Pevey, Jason P. Hayward, Glenn O. Allgood

Accepted for the Council:
Carolyn R. Hodges

Vice Provost and Dean of the Graduate School

(Original signatures are on file with official student records.)

A Bayesian Approach to Broad-Area Nuclear and Radiological Search Operations

A Dissertation Presented for the

Doctor of Philosophy

Degree

The University of Tennessee, Knoxville

Samuel James Willmon

May 2014

Dedication

For my wife, without whom I would be lost, and my parents who set me on the path to explore the world around me.

Acknowledgements

I would like to thank Dr. Howard Hall for not only serving as my research advisor, professor, mentor, and friend, but also for his dedication to educating and training the next generation of nuclear security professionals. Dr. Hall epitomizes the Army methodology of teaching, coaching, and mentoring when it comes to his students. I would also like to thank Dr. Hall for giving me the latitude to explore the bounds of the broad-area search problem and the guidance needed to keep me focused. I am deeply indebted to my committee members who not only taught or reminded me of the fundamentals during course work, but also for the support they provided while I wrestled with the complex issues that plague the broad-area search problem space. I would also like to thank Dr. Allgood for the sanity checks he provided throughout this endeavor. His motivation always provided me with the reinforcement and focus that I needed in order to overcome any doubt that a solution exists within a Bayesian framework.

At the University of Tennessee, I am thankful for the help and support from our research group. Particularly, I would like to thank: Matt Cook for his never ending supply of MCNP tips and tricks as well as his work to keep the computers running; Hannah Hale and James Ghawalry for their work in tackling their respective pieces of the puzzle; and, my brothers in arms for keeping some levity in the office.

I would be remiss if I didn't thank my friends, colleagues, and expert advisors at the Oak Ridge National Laboratory. Their support and guidance helped vector me in on numerous occasions and provided me with alternate perspectives.

I am most thankful for the love and unwavering support from my wife throughout this entire process. Her never-ending patience, understanding, and single-minded focus in ensuring that we accomplish this mission on time has been the bedrock of any successes I can claim. While the work and words herein are mine, the past three years has truly been a team effort.

Abstract

This dissertation describes the development, implementation, and initial performance testing of the Broad-Area Search Bayesian Processor (BASBP). The BASBP is a novel FORTAN code designed to combine the data from aerial radiation detection platforms with available geo-spatial data using Bayesian techniques to provide updated parameter estimates of the problem space. By employing empirical fits to the Monte Carlo photon flux estimates generated using MCNP6, the core BASBP model accounts for the increasing significance of photon scattering and absorption events with source-detector range. The BASBP employs Bayesian signal processing methods to estimate both the spatially varying background and the most likely signal contribution from radioactive sources of interest. In demonstrating the capabilities of the BASBP, it is shown that the coupling of Bayesian signal processing methods with radiation transport physics affords the opportunity to effectively treat the spatially varying background signal, improve the range at which detection, localization, and identification decisions are made; provide real-time recommendations on sensor employment; provide the framework for fusing data from multiple sensors and data from disparate sensor types (true multi-source data fusion); and, enhance the nuclear detection capabilities of first responder or national security organizations.

Table of Contents

List of Tables

List of Figures

1 | Introduction

For the better part of a decade, the United States government has identified the lack of a broad-area search capability as a critical gap in the nation's ability to counter the spread and/or use of nuclear and radiological weapons. The research described examines two essential questions: (1) can Bayesian signal processing methods significantly increase the range at which radioactive source detection, localization, and identification decisions are made?; and, (2) can Bayesian methods provide a framework for fusing technical data with disparate data sources and data types in order to increase situational understanding of the search space? While the former serves as the focal task from a nuclear engineering perspective, the latter offers the potential to substantially change current opinions of how localized detector data nests within the larger operational context. Two fundamental principles serve to justify the pursuit of an alternative approach to the broad-area search problem: the importance and persistence of the operational need; and, the technical challenges confronting the current suite of state-of-the-art technologies that employ traditional approaches to the problem.

1.1 Justification

While detailed requirements tend to be tightly controlled, several senior-level references within the Department of Defense illuminate the importance of the required broad-area search capability. The 2006 Quadrennial Defense Review (QDR) Report stated that "preventing state or non-state actors from acquiring or using [Weapons of Mass Destruction] highlights the need for...capabilities to detect fissile materials such as nuclear devices at stand-off ranges" [1]. The QDR of 2010 addressed the stand-off detection capability shortfall in more specific terms by directing the Defense Department to "accelerate the development of standoff radiological/nuclear detection capabilities" [2]. The "DoD will improve its ability to detect radiological and nuclear material and weapons at a distance. Developing and fielding these sensors will make possible more effective wide area surveillance in the maritime and

air approaches to the United States, and will help address the challenge of locating and securing nuclear weapons and materials during overseas contingencies" [2]. Concurrent with the department's work on the 2010 QDR, a report by the Government Accountability Office highlights the fact that the combatant commanders (the most senior admirals and four-star generals in the armed services) identified stand-off detection as one of the key shortfalls in the Joint Staff's 2009 Combating WMD Strategic Global Assessment [3].

In terms of desired capabilities, the U.S. Army's Training and Doctrine Command* has articulated the Army's goals with respect to multi-sensor data fusion in *The United States Army Concept Capability Plan for Combating Weapons of Mass Destruction for the Future Modular Force, 2015–2024* [4]:

> [H]olistically the Army must possess the capability to gain [situational understanding] by fusing such things as human intelligence, signal intelligence, and document exploitation with traditional technical sensor inputs... Sensors will include layers of [joint, interagency, intergovernmental, and multinational] assets; point and standoff sensors; and static, mobile and remotely emplaced sensors; as well as intelligence feeds. Mobile sensors include Soldiers and sensors mounted on a variety of platforms including Soldiers, manned platforms, and unmanned ground and aerial platforms. Disparate (non-CBRN† specific) sensors will compose another layer. Their purpose is to provide additional indicators to increase the level of confidence in detections by other sensors or to cue CBRN sensors and other disparate sensors to focus their search area.

The broad-area search capability gap is not unique to the Department of Defense. In July of 2012, the acting director of the Domestic Nuclear Detection Organization (DNDO) within the Department of Homeland Security made the following statement to the U.S. House Committee on Science, Space and Technology: "While DNDO's work to develop, evaluate,

*The U.S. Training and Doctrine Command is charged with the responsibility for educating and training the Army's Soldiers, civilians and leaders; supporting unit training; and designing, building and integrating a versatile mix of capabilities, formations, and equipment to strengthen the U.S. Army.

†CBRN is the military acronym for Chemical Biological Radiological Nuclear

and deploy systems supports the ongoing enhancement of the [Global Nuclear Detection Architecture], significant technical challenges remain. These challenges include:...[e]nhanced wide area search capabilities in a variety of scenarios to include urban and highly cluttered environments" [5].

Strategic statements and the Army's conceptualization of desired future capabilities do not highlight the fact that at this very moment, elements across the U.S. government are prepared to conduct a broad-area search for radioactive material. Despite the fact that the operational employment of current state-of-the-art technologies utilize a localized approach, elements within the U.S. Departments of Defense, Energy, Homeland Security, and Justice have no choice but to respond to potential threats with the equipment at hand. The operations of the U.S. Army's Nuclear Disablement Teams during Operation IRAQI FREEDOM serve as one example in which operational units have had no choice to but to employ radiation detection systems without a broad-area search capability [6].

1.2 Literature Review

Bayesian signal processing methods have a well-established presence in the fields of radar and sonar tracking, and are increasingly employed in problems related to robotic sensor guidance, wireless signal mapping, and image processing/object tracking. To date, little effort has been made to utilize Bayesian signal processing methods in the field of radioactive source detection. A canvassing of published research reveals a small body of published work related to this effort.

1.2.1 Radiation Portal Monitoring Applications

Researchers at the Lawrence Livermore National Laboratory (LLNL) successfully demonstrated a Bayesian processor applied to the case of a stationary portal monitoring system. Using a photon-by-photon discriminator, J.V. Candy's team demonstrated the ability to detect radioisotopes of interest in the presence of constant, uncharacterized background

sources. While their latest published work (2011) describes the inclusion of a Compton-scattering discriminator which accounts for scattering events occurring within the detection system, Candy's team has not addressed radiation transport phenomena which occur between the source and detector. Given the context of their work and the physical dimensions of the problem-space considered, inclusion of radiation transport phenomena taking place between the source and detector could serve as a means to address the presence of shielding materials within the problem geometry [7]. Following the methods developed by LLNL, Chinese researchers at the China Academy of Engineering Physics revalidated the Bayesian approach in 2013 [8].

Also in an effort to tackle the stationary portal monitoring system from a probabilistic approach, a team of researchers at the Pacific Northwest National Laboratory (PNNL) published their work in 2011 which focused on coupling adjoint radiation transport considerations and detector response data within Bayesian framework in order to infer the presence of radioactive materials within containerized cargo [9]. As with the work performed by LLNL, the PNNL team did not consider the case of an unknown or spatially varying background or extend the utility of their approach to mobile applications.

1.2.2 Operational *Local* Search Applications

In a series of papers culminating in 2010, researchers at the Defense Science and Technology Organization (DSTO) and the University of Melbourne in Australia demonstrated their Bayesian approach to the operational *local* search for radioactive sources. Employing a Bayesian particle filtering method, the DSTO team demonstrated the ability to localize a radioactive source within the search area as well as guide the employment of detectors during the search. The mathematical model presented by DSTO only accounted only for the spherical divergence of the photon signal and assumed a known and constant background (9 orders of magnitude below the strength of the radiation source employed) [10]. While demonstrative of the Bayesian concept, the DSTO model is ill-suited for the broad-area search environment.

1.3 Research Objectives

As previously introduced, this research seeks to advance the state of the art of radiation detection. Specifically, the operational utility of Bayesian signal processing methods in the context of the broad-area search for radioactive sources is examined. Central to this research is the question of whether or not Bayesian methods offer the means to extend the range at which detection and localization decisions are made. The central problem is deconstructed into the following tasks:

1. Characterize the broad-area search problem. This task defines the central parameters that impact the broad-area search for radioactive sources.

2. Investigate the photon signatures of radioactive sources of interest. Developing a means to detect radioactive sources from a distance requires an understanding of the signals such a system is expected to find. Second, the practical limits to the distance travelled by photons of interest must be identified.

3. Identify problems with applying current approaches at extended ranges. This task centers on the root question of whether or not an alternative approach is needed.

4. Develop a Bayesian signal processing model that overcomes the identified weaknesses of traditional detection models.

5. Develop a Bayesian processor that integrates the functions required to detect and localize radioactive sources at extended ranges. The Bayesian processor developed in this step will also provide the backbone for the future development of a real-time, sensor guidance module and provide the framework for fusing information streaming from radiation detectors with disparate data sources.

6. Demonstrate the Bayesian processor. Given radiation survey data collected in the field, this task tests the performance of the Bayesian processor.

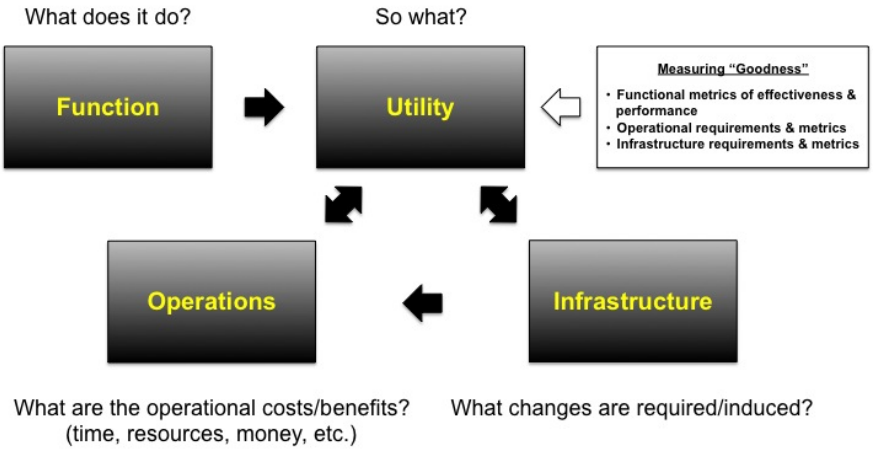

Figure 1.1: Assessing the impact of technology on operations.

With the goal of providing an operationally viable tool capable of generating real-time detection, localization, and guidance information, the BASBP leverages the parallel processing capabilities of modern laptop computers by implementing the algorithms in modern FORTRAN and using multi-threaded processes to significantly increase execution speeds.

The anticipated contributions of this research to the operational search community fall into four categories (as depicted in Figure 1.1): function, operations, utility, and infrastructure. In terms of function, irrespective of the radiation detector type or platform, this research focuses on fundamentally altering the analytical processes used to interpret radiation detector data. The combination of Bayesian signal processing methods and radiation transport physics offers the means to increase the range at which source detection and localization decisions are made. Operationally, the employment of a Bayesian approach to the broad-area search problem fundamentally alters current methods. First and foremost, an increase in the range of detection and localization has the immediate effect of reducing the resources required to search a given area. Second, real-time data analysis and sensor guidance allows the operational team to maximize the allocation of resources. And third, the anticipated Bayesian processor will provide the means for real-time data fusion, unlike conventional radiation survey analysis which is habitually incompatible with the data and

analytical products from disparate sources. In terms of utility, the direct application to radiation detection systems are clear. However, approaches developed in the course of this research to deal with variable background noise and low-SNR environments may have applications in other technical fields as well. The employment of a Bayesian processor will not significantly effect the infrastructure required by operational search teams.

1.4 Dissertation Outline

This dissertation is organized into chapters that group the contents by function. Chapter 1 serves as the introductory chapter and provides the background and motivation behind this research. Chapter 2 provides an operational perspective of the broad-area search problem that includes the characteristics of the problem, dimensionality and parameters of interest. To shed further light on the nature of the operational search problem, a discussion of the photon signatures associated with materials of concern is presented. Issues facing conventional detection systems when confronted with the broad-area search challenge are introduced. The mathematical framework required for development of the Bayesian signal processor is presented in Chapter 3. This includes a description of the Bayesian approach to signal processing and the theoretical framework for one of the most common Bayesian methods, the particle filter. Chapter 4 contains the detailed development of the following primary processes used by the BASBP: selection of the *prior* distributions; estimating of the local background signal; the detection decision; updating the *posterior* distribution; data fusion. Anticipating the continuation of this research, Chapter 4 concludes with a proposed a way ahead regarding the implementation of a sensor guidance component. Chapter 5 presents the results of testing the BASBP given background data collected from aerial platforms injected with source signal based on MCNP modeling. Finally, the conclusions drawn from this research are presented in chapter 6, along with recommendations for continued examination of the Bayesian approach to the broad-area search problem.

2 | Scoping the Broad-Area Search Problem

2.1 Introduction

The objective of the broad-area search* mission is the detection, localization, and when possible, the identification of sources of radiation that pose a threat to the public. *Detection* refers to the binary decision of whether or not a source exists within range of the detection system. The term *localization* refers to the subsequent geolocation of the radiation source. While detection and localization must occur before recovery operations can begin and the radiation source moved to its final disposition location, some radiological search platforms perform both steps in tandem. However linear the approach may appear, wide-ranging uncertainties cloud the characteristics that define the broad-area search problem.

This chapter begins with the characteristics of the broad-area search problem space. With an understanding of the scope of the problem and the primary interest in detecting and localizing gamma sources at the maximum range possible, the photon signatures of interest are identified along with the associated practical limits to the ranges at which they propagate in air. Following the discussion of photon signatures and ranges, a brief overview of the challenges of employing current detection systems in the context of broad-area search operations is provided. An outline of the critical assumptions imposed on the broad-area search problem concludes this chapter.

2.2 Characteristics of the Broad-Area Search Problem

The broad-area search problem begins with the recognition that a radiation source poses a potential threat to the public. The level of detail in the information triggering the broad-area search ranges from general to very specific. Factors suggestive of a potential radiological

*As applied to search for radiological sources, the ill-defined term *broad-area search* generates significant discussion. In general terms, the lower bound of the dimensions of broad-area search problems exceeds hundreds of square meters.

problem may include: the reported loss or theft of sources by licensed users; patients seeking treatment for radiation-induced sicknesses at medical facilities; data collected from fielded detection systems; and, information suggestive of a nuclear/radiological terrorist threat. Characteristics that define the the broad-area search problem include:

- the nature of the radiation source (material form, isotope, and activity);
- the circumstances triggering the search (loss or theft of rad source, terrorist threat);
- the packaging/shielding materials surrounding the source;
- the mobility of the source;
- the presence of spatially & temporally varying background radiation;
- the amount of time elapsed since the loss or theft of the source;
- the size of the search area;
- the geo-spatial environments contained within the search area.
- the range at which available search platforms detect radiation; and,
- the number of search platforms available.

Of these, the four most significant challenges facing current mobile detection systems are: the presence of packaging/shielding materials, time-distance relationships impacting the size of the search area, the variable background radiation, and detection ranges. While nearly all plausible scenarios involve some form of packaging and shielding materials, this study focuses on the limits of detection in the un-shielded case. The argument for doing so is three-fold. First, the combination of potential shielding/packaging materials exists as a near-infinite set of scenario-dependent possibilities. Second, should the shielding material prevent any passive radiation signature from escaping the configuration, no amount of technology gains in the field of passive radiation detection will suffice. And third, an increase in the range of the detection of unshielded photons implies a corresponding increase in the range at which detection systems can detect photons scattered by shielding materials.

To illustrate the challenge of time-distance relationships, Figure 2.1 depicts the geometric growth of the search area following the notional theft of a radiation source from the University of Tennessee campus in Knoxville. Assuming that the perpetrators flee the scene by vehicle,

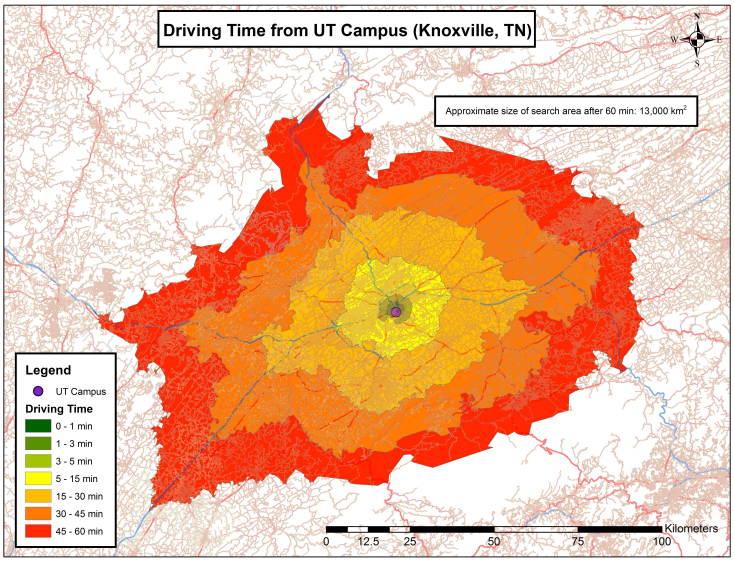

Figure 2.1: Time-based growth of potential search area following notional theft from UT campus.

analysis of the surrounding road system using data from the U.S. Census Bureau [11] and ArcGIS® software suggests that after 60 minutes, the search area grows to approximately 13,000 km^2. To search an area of this size without specific information and while equipped with short-ranged detection instruments is a futile proposition.

The development of solutions to the broad-area search problem requires first an understanding of the materials most likely to pose a threat. Second, when confronted with the proverbial challenge of finding a needle in a haystack using passive techniques, one must know the signatures emanating from the materials of interest. The third key element required to scope the broad area search problem is knowledge of the extent to which the signatures propagate and are available for detection. The sections that follow examine photon sources, their signatures, and their corresponding ranges in air.

2.3 Identifying Photon Signatures of Interest

The emission of radiation by an atom following radioactive decay serves as an identifying feature unique to each isotopic species and is characterized by the emission type, energy and

frequency. Radioactive materials of concern (MOC) fall into one of two general categories: conventional radiation sources that could be used in a radiological dissemination/dispersal or exposure device (RDD or RED); and, Special Nuclear Material (SNM) suitable for use in nuclear fuel or other components. Out of the more than 3,300 known radioactive isotopes, only a relatively few have commercial or industrial uses or are required for nuclear weapons. The examination of photon signatures begins by drawing attention to those isotopes most commonly used in commercial, industrial, or weapons applications. Further refinement of the list of candidate MOC is made possible by analyzing information from the IAEA regarding those isotopes most commonly reported in radioactive source incidents.

2.3.1 Identifying Material of Concern

Radioactive sources have a broad range of applications – from relatively weak Am-241 sources found in common smoke detectors to extremely intense industrial sources used in industrial sterilization machines. Table A.1 in Appendix A lists the common uses of conventional radiation sources, the activity levels typical of the method of use, and the IAEA's hazard category. While SNM categorically contains a broad range of mixtures of isotopes, the investigation herein focuses on the relative extremes: depleted uranium (DU), highly-enriched uranium (90% U-235 content), and weapons-grade plutonium (>90% Pu-239 content). The sources that pose the greatest threat to life (IAEA categories 1–3) have applications in industrial radiography, nuclear medicine, and in radioisotope thermoelectric generators. In 2005, the IAEA summarized the radiological source incidents reported by member states for inclusion in the Illicit Trafficking Database (ITDB). Figure 2.2 depicts the relative frequency of sources of radiation involved in the reported incidents [12].

Combining the IAEA Category 1–3 sources with the historical perspective suggested by the IAEA's 2005 Illicit Trafficking Database summary, the following gamma-emitting sources of radiation serve as the focus of attention:

- **Conventional sources:** Co-60, Se-75, Cs-137, Ir-192, Ra-226, and Pu-238.
- **Special Nuclear Materials:** DU, HEU, HEU (with trace U-232), and WGPu.

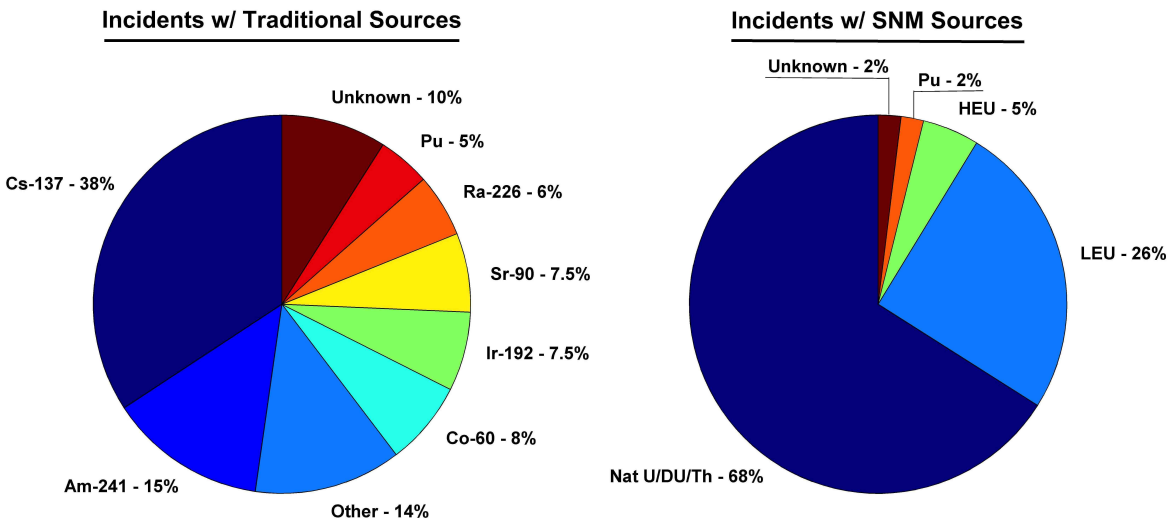

Figure 2.2: Incidents involving radiation sources 1993-2005 as recorded in the IAEA's Illicit Trafficking Database.

2.3.2 Photon Signatures of MOC

Based on the data provided by the National Nuclear Data Center [13], over 1,900 photons are associated with the radioactive decay of MOC, considering both gamma- and x-rays and accounting for competing decay chains. Analysis of the data indicates that the bulk of the photon signatures for MOC resides in the 0.1–0.8 MeV range. Only a select few materials of interest have photon signatures in the 1.0–3.0 MeV range (i.e.: Co-60, HEU contaminated with trace amounts of U-232, and DU). Table A.2 lists the five most prominent photons with an initial energy of 0.1 MeV or greater emitted by each of the conventional sources of radiation. Figure 2.3 depicts the spectrum of photons emitted by conventional sources against the backdrop of the mean free path (MFP, the average distance traveled before interacting with a material) of the photons in air.

While identifying a unique isotopic species from the spectrum of photons emitted is a straightforward process, uncertainties in identifying the photon signatures associated with SNM arise due to variable production methods, purity levels, and uncertainties associated with the amount of time elapsed since production. As an example of differing signatures based on production methods, consider the case in which uranium is reprocessed following

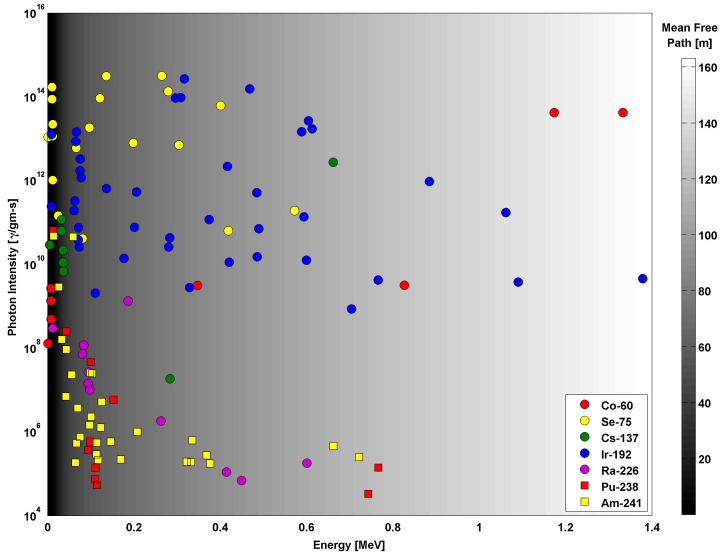

Figure 2.3: Photon intensity and mean free path in air as functions of photon energy for isotopes of concern.

irradiation in a nuclear reactor. Normal reactor operations produce trace quantities of U-232 evident in the post-irradiation fuel elements. If the fuel is reprocessed to recover the remaining uranium and then further enriched, the U-232 will preferentially follow the lower-mass U-235. Indicative of the signatures associated with generic forms of SNM, Table A.3 lists the five most prominent photons with an initial energy of 0.1 MeV or greater emitted by each SNM-type considered, where the SNM has been aged 5 years. Figure 2.3 depicts the estimated spectra emitted by each type of SNM. The complexity of the spectra stems from the variety of photons emitted by the decay chains associated with each parent. While uncertainties abound regarding the expected intensity of each decay chain, the ratios between key photon intensities may suggest the presence of SNM when a spectrum collected is particularly cluttered.

While the Tables A.2 and A.3 provide the primary signatures associated with MOC, the following observations generalize their characteristics:

- The photon intensity and relative frequency for emanations from convention MOC are well known;

- The photon signatures from SNM sources are unique to the production method and materials used. However, the relative occurrence of isotopic signatures can suggest an increased likelihood of SNM.
- With few exceptions, the photon energies of interest are below 0.8 MeV. Exceptions include emissions from: Co-60, Tl-208 (daughter product in the decay chain of HEU contaminated with U-232), and Pa-234 (daughter product in the decay chain of DU);

2.4 Identifying the Physical Limits of Photon Ranges

Advances in nuclear detection technologies tend to focus on improvements in energy resolution and detection efficiencies—efforts largely aimed at enhancing the sensitivity and precision of detection systems. However, the broad-area search for radioactive sources must come to terms with the physical limit to the range at which photon signatures exist in detectable quantities. While the optimization of a detection system (as defined by parameters that characterize a detection system describe the system's ability to convert a known photon flux into the electronic impulse signals recorded) clearly enhances system performance, system optimization does not address the fundamental question of photon range.

The Monte Carlo Neutral Particle transport code (MCNP6.1, [14]) readily produces estimates of the range of photons in air. As a simple test case, consider a notional Cs-137 point source surrounded by spherical volumes of air. By requiring that MCNP tally the photons as they pass thru each surface, MCNP estimates the flux by dividing the photon tally at a surface by the surface area. Figure 2.4a depicts a generic representation of an MCNP tallying surface. Of note, the generic flux tally in MCNP is independent of the photons' direction of travel as they cross the tally surface. Figure 2.4b shows the resulting estimated energy distribution of the photon flux from a Cs-137 source at ranges extending from 1m – 1,000m.

By running 1E9 Monte Carlo particles in the simulation, except for the extremely low energy bins of the 500 m and 1,000 m runs, the variance of the estimated flux is less than 2%. The first important conclusion drawn from Figure 2.4b is that while an argument can

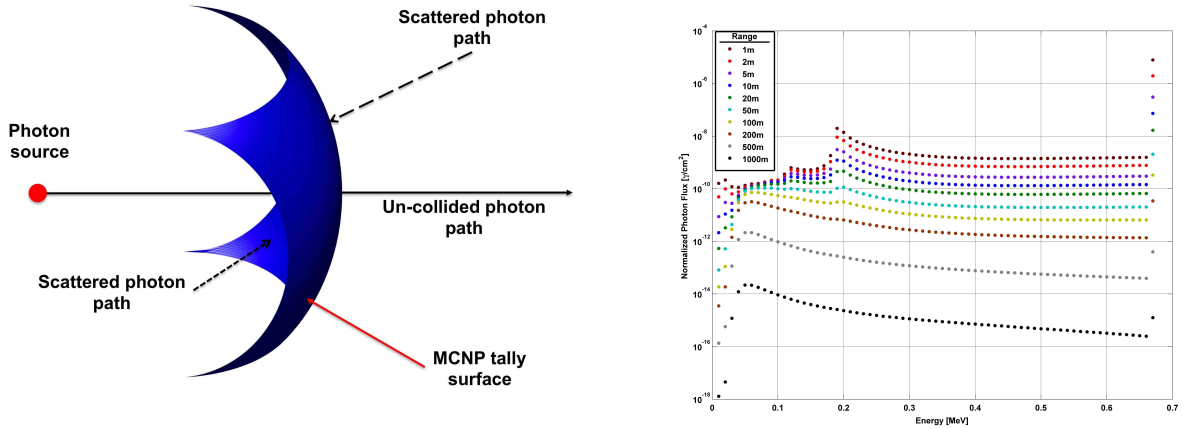

(a) Depiction of tally surface used by MCNP flux estimations.

(b) Estimated photon flux vs Energy for Cs-137 in air.

Figure 2.4: MCNP photon flux estimation.

be made that photons from a Cs-137 source can reach 1 km in range with some probability greater than zero, the practical limit to the range of Cs-137 photons most likely exists within the range between 200 m and 500 m. This observation is based on the fact that the variance of the flux estimates decreases up to the point where the source-detector range exceeds 200 m (see Figure A.2).[†] The second important conclusion suggested by the data is that as the source-detector distance increases (photon range), the contribution of photons below the full energy peak to the total flux reaching the surface of a detector also increases and eventually surpasses the contribution made by photons in the full energy peak. Figure 2.5 shows that the cross-over point (scattered photons make up the majority share of the total flux) occurs at approximately 50 m for photons originating from Cs-137. Cast in terms of the MOC signatures, this means that the greater the source-detector distance, the less the photon signature at that distance resembles the discrete energy lines with which they were born.

[†]No claim is made regarding the ability of detection systems employing Bayesian signal processing methods to detect photon emanating from Cs-137 at a distance of 200m or more. The point highlighted here is the fact that the population of photons from Cs-137 begins to exponentially decay at approximately 200 m — significantly reducing the probability of detection at ranges beyond 200 m.

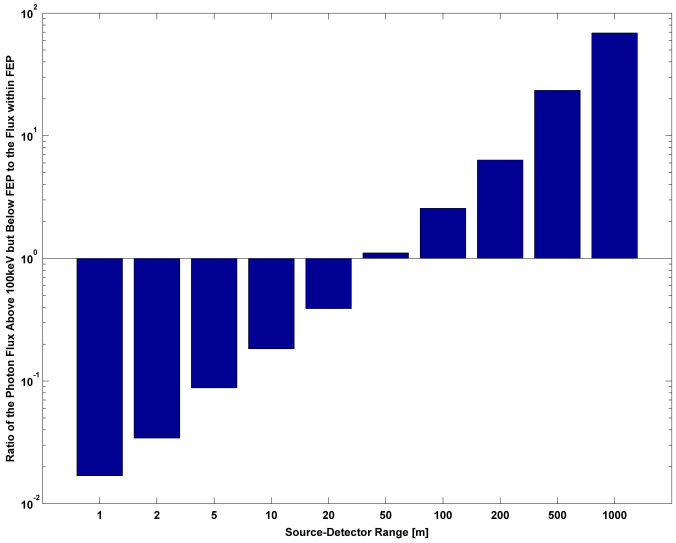

Figure 2.5: Photon flux ratio (below / within FEP) as a function of source-detector range.

2.5 Challenges Applying Conventional Detection Systems in a Broad-Area Search Role

The introduction at the beginning of this chapter listed the characteristics of the broad-area search problem. This section focuses on the challenges confronting conventional detection systems when employed in a broad-area search role. Conventional radiation detection systems typically fall into one of four categories: gross-counting systems, spectroscopic systems, gross-counting imaging systems, and spectroscopic imaging systems [15]. The general characteristics of each type of detection system include:

- **Gross-counting systems:** The most basic of all radiation detection systems, gross-counting systems simply record the number of interaction events that occur within the detector's sensitive volume as a result of incident radiation. The only parameters available for detection and localization decisions are the gross counts and the count rate (gross counts divided by the measurement time). Such systems require a prior

measurement or estimate of the background radiation to make a detection decision and attribute any portion of the measured counts to a potential source of interest.

- **Spectroscopic systems:** Unlike gross-counting systems, spectroscopic detection systems record tallies of the radiation-induced events in discrete energy bins. Therefore, these systems are able to provide a spectral distribution of the events recorded over the measurement period. Spectroscopic detection systems can provide an estimate of the number of sources present as long as the sources have distinct emissions.
- **Gross-counting imaging systems:** In gross-counting imaging detection systems, a recorded event includes spatial and/or angular information with respect to the detection system's sensitive volume. This information can be used to estimate the number and spatial distribution of sources in the detector's field of view.
- **Spectroscopic imaging systems:** Similarly, spectroscopic imaging systems record the spatial and spectral history of the events registered. These systems can estimate the number, spatial distribution, intensity, and types of sources within the detector's field of view.

With these general properties in mind, the challenges with employing traditional detection systems in a broad-area search role fall into three categories: the manner in which they treat the background signal in order to reach a detection decision; the physical model used to localize potential radiation sources; and, the operational method of detection and localization. Each of these topics is covered in greater detail in the following sections.

2.5.1 Limitations Imposed by Treatment of the Background

When confronted with a detection decision, systems must decide whether or not the measured signal contains some portion attributable to a source other than the local background. Given that the magnitude and spectral content of the background signal varies both temporally and spatially, conventional detection systems typically require either a prior measurement or a fairly accurate estimate of the background in order to decide if the current measurement indicates the presence of a source of interest. In recent years, research and technology

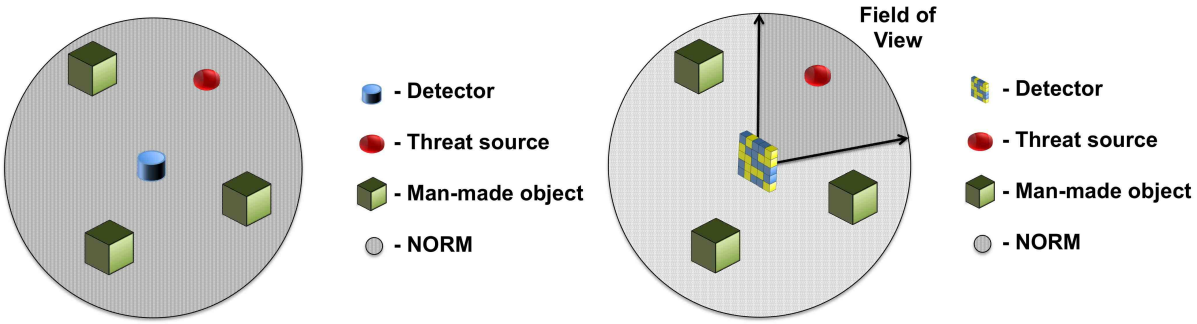

(a) 4π detector scene. **(b) Imaging detector scene.**

Figure 2.6: Comparison of notional detector scenes.

demonstrations have significantly advanced the application of imaging detection systems in the area of nuclear and radiological search problems. [16]–[22]. Due to their ability to systematically remove the background signal from the observed signal, imaging systems typically outperform non-imaging systems when challenged with point sources at extended ranges.

Figure 2.6 (adapted from K. Vetter's guide to imaging systems [20]) compares the notional scene observed by a 4π detector to that of a generic imaging detector. As depicted in 2.6b, imaging detectors can significantly reduce the background contribution to the measured signals. However, the benefits of reducing the background signal diminish as the source-detector distance increases. As previously shown in Figure 2.5, the down-scattered flux from sources of interest make up an increasing share of the total flux at ranges beyond 50m. With the increased importance of the scattered flux component in mind, the following systemic properties reduce the effectiveness of imaging detection systems in broad-area search operations:

- The shielding that limits the scene to the detector's FOV also prevents scattered source photons from reaching the detector;
- Use of a coded mask prevents as much as 50% of the incident flux from reaching the detector;
- Some imaging techniques filter the response signal according to regions of interest centered on the full-energy peak(s) of sources of interest; and,

- The deconvolution methods used to remove the background signal interpret much of the scattered source signal as background.

2.5.2 Use of Ill-suited Localization Models

The process of estimating the geo-spatial location of a radiological source based on the data collected by radiation detectors requires a physical model that relates the observed measurements to a point or points in space. The Boltzman transport equation (BTE), given in generic form by Equation 2.1, offers the most complete representation of the physical phenomena that occur between source particles streaming from their point of origin and the measurements recorded by a detector [23], [24].

$$\frac{1}{c}\frac{\partial\Psi(\vec{r},\vec{\Omega},E,t)}{\partial t}+\vec{\Omega}\cdot\nabla\Psi(\vec{r},\vec{\Omega},E,t)+\sigma_t(\vec{r},E,t)\Psi(\vec{r},\vec{\Omega},E,t)=q(\vec{r},\vec{\Omega},E,t) \tag{2.1}$$

where $\Psi(\vec{r},\vec{\Omega},E,t)$ is the position-, direction-, energy-, and time-dependent angular flux of particles, σ_t is the location-, energy-, and time-dependent total interaction cross-section, $q(\vec{r},\vec{\Omega},E,t)$ represents the location-, direction, energy, and time-dependent production of particles, and v is the speed of light. The first term in Equation 2.1 clearly represents the time rate of change in the angular flux. The spatial divergence of the angular flux is represented by the second term. The total interaction cross-section in the third term carries the information required to estimate particle losses due to collisions. Particle production, represented in the final term, q, consists of the sum of all external particle sources and the particles generated by the interaction of radiation with matter.

In the context of the broad-area search problem, one generally seeks the relationship between the flux incident upon the surface of a detector (which directly relates to the detector's response) and the fixed, point sources of radiation. Assuming that the physical system is in steady-state and the material properties of the system do not evolve with time, one can readily drop the the first term and remove the time dependence of the remaining terms of the BTE. While fairly simple in form, in most practical situations, solutions to the BTE do not exist in closed form as the production and loss terms are tightly coupled by the

angular flux. Additionally, solving the BTE requires detailed knowledge of the distribution of materials and sources of radiation (as well as the physical properties of both) throughout the problem space. Consequently, approximations to the BTE are generally required — most often through Monte Carlo or finite element methods.

Due to time constraints and the range at which detection decisions are made, localization models typically apply what is known as the $1/r^2$ approximation. Simply put, this approximation ignores the interaction of radiation with matter and relates the observed flux $\mathcal{I}$ at location $\mathbf{x}_d$ to the source intensity $\mathcal{I}_0$ at location $\mathbf{x}_s$ and inverse of the square of the source-detector distance, $r(\mathbf{x}_d, \mathbf{x}_s)$, as expressed in Equation 2.2. Physically, this approximation represents only the spherical divergence of the radiation as it propagates outward from a point source.

$$\mathcal{I}(\mathbf{x}_d) \propto \frac{\mathcal{I}_0(\mathbf{x}_s)}{4\pi r^2(\mathbf{x}_d, \mathbf{x}_s)} \tag{2.2}$$

Similar to the issues raised regarding the methods used in conventional detection systems to grapple with the background signal, recall the conclusion drawn from basic MCNP modeling that photon interaction mechanisms dominate the BTE at extended source-detector ranges. Therefore, as shown in Figure 2.5, the $1/r^2$ approximation fails to adequately predict the expected photon intensity at extended ranges. Connecting concerns with the background treatment, this proposition can be cast in terms of the signal-to-noise ratio (SNR). SNR values serve as a quantifiable metric of the threshold for detection decisions. From the fundamentals of counting statistics, the SNR for a generic counting system (given a long-lived source and time-invariant background) is given by: $\text{SNR} = S/\sqrt{T+B}$, where S represents the counts due to the source of interest, T is the sum of the source and background counts, and B is the number of counts due to the background alone [25].

Consider the case of a 1 mCi Cs-137 point source, an ideal detector with an area of 100 cm^2 conducting measurements a a variety of known locations, and the background flux is fixed at $1\frac{\gamma}{cm^2 \cdot s}$. Figure 2.7 depicts the estimated flux and SNR values generated from MCNP modeling as compared to the values obtained using the $1/r^2$ approximation. Based on the data represented, the following conclusions may be drawn:

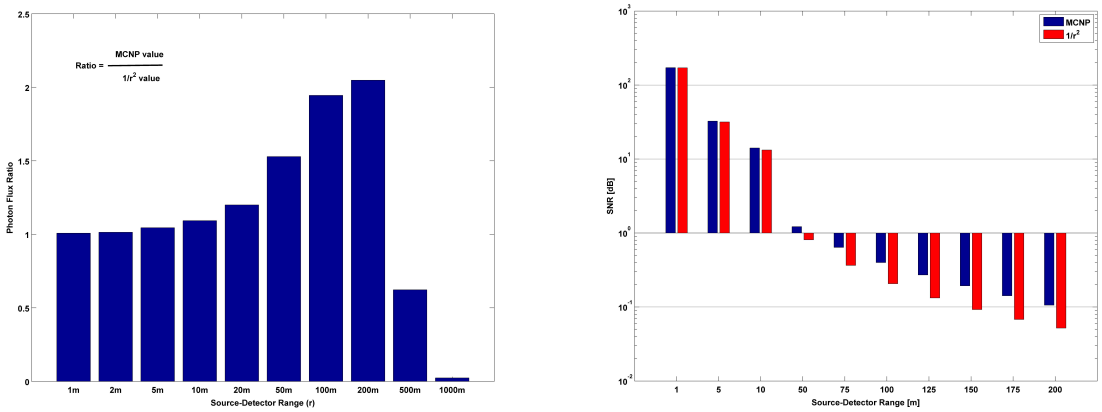

(a) Ratio of flux estimates. **(b) Estimated SNR values.**

Figure 2.7: Comparison of MCNP and $1/r^2$ estimates of photon flux and SNR values.

- The importance of photon scattering events increases until the absorption of photons dominates the transport process (at approximately 150 m for Cs-137 photons);
- At ranges beyond 200 m, the $1/r^2$ approximation over-estimates the photon flux; and,
- Under-estimation of the SNR value at extended ranges may lead to false conclusions regarding the availability of a potential source signal.

2.5.3 Use of an Un-informed Operational Search Pattern

The final observation made regarding the application of conventional detection systems in broad-area search scenarios deals with the operational manner in which these systems are employed. In short, operational approaches to the broad-area search for radioactive sources has not significantly changed in decades. While scientific advances have greatly expanded the range of technologies available via man-portable and ground-, sea-, and air-based platforms, the broad-area search remains largely tethered to the gridded survey approach. The comparison of the aerial survey methods used during an exercise of European emergency response teams conducted in 2001 (Barents Rescue 2001 LIVEX) to those used by the Department of Energy's Remote Sensing Laboratory (RSL) Aerial Measuring Systems (AMS) finds that both consist of the following common elements [26], [27]:

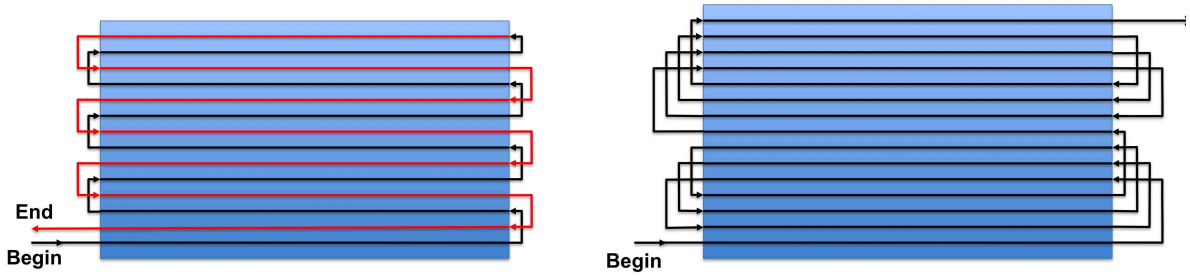

(a) Down & back pattern. **(b) Repeated loop pattern.**

Figure 2.8: Examples of aerial gridded-search flight patterns.

- Objective altitude: 50-100 m
- Grid spacing: 100-200 m
- Ground speed: 100-200 km/h
- Detection system: Spectroscopic (non-imaging)
- Integration (sampling) time: 1 s
- Data processing: count rate and spectral data is available in real-time; contextual analysis requires post-processing

Given the common traits, operational employment of aerial detection platforms is executed in the form of overflying the search area using a gridded search pattern. Figure 2.8 depicts examples of commonly used patterns. Factors impacting flight pattern selection include: the time available and crew, aircraft, and detection system performance. While both patterns shown provide coverage of the notional search area using the same number of turns, the repeated loop pattern shown in Figure 2.8b highlights the impact complicated flight patterns can have in terms of the distance traveled/time spent outside of the search area.

While real-time sensor guidance is not feasible for fixed-wing detection platforms such as the Swedish Shrike Commander (mounted with a downward-looking 16,800 cm^3 NaI detector and an upward-looking 4,200 cm^3 NaI detector) [27], the benefits of real-time sensor guidance are clear.

2.6 Critical Assumptions

This chapter concludes with the critical assumptions imposed on the broad-area search problem. Given the general characteristics of the problem and associated wide-ranging uncertainties, the objective here is to refine the problem space such that the development of the Broad-Area Search Bayesian Processor follows with a sense of clarity. Table 2.1 lists critical assumptions, grouped according to the primary parameter impacted. While the validity of some of the assumptions is self-evident (such as placing bounds on the spatial domain), some assumptions are made solely out of convenience in order to provide a focus for this research (such as narrowing the scope to gamma-emitting sources). Further discussion of the critical assumptions occurs where they apply to the development of a specific component of the BASBP.

Table 2.1: BASBP Critical Assumptions

Number	Topic / Assumption
1.0	**Radiation Source**
1.1	The source is a γ-emitting point source.
1.2	The source is stationary ($v_{x_s}, v_{y_s}, v_{z_s} = 0$).
1.3	The source is unshielded.
1.4	The estimated source strength, $\mathcal{A}_s$, is bounded ($\mathcal{A}_s \in [\mathcal{A}_{\min}, \mathcal{A}_{\max}]$).
1.5	The source is restricted to the surface of the ground (z_s = local elevation).
2.0	**Search Space**
2.1	The spatial limits are restricted to $[x_{\min}, x_{\max}]$ and $[y_{\min}, y_{\max}]$.
2.2	The search begins in a location clear of potential sources of interest.
2.3	The duration of the search, Δt, is much shorter than the half-lives of sources of interest ($\Delta t \ll \lambda_s$).
2.4	The minimum set of geo-spatial data exists.
2.5	The background radiation varies with land-use category.
3.0	**Detection Platform**
3.1	The characteristic parameters, $\mathcal{D}_{det}$, are known.
3.2	Systematic noise in the measurements from the detection platforms is much smaller than the variations due random decay and transport processes.

3 | Bayesian Signal Processing Framework

The operational, broad-area search mission relies on the ability to detect the presence of a radioactive source (or multiple sources), localize the source(s) in space, and if possible identify or classify the source(s) based on measurements collected by radiation detection systems. The broad-area search problem begins as a classic Bayesian inference problem: what inferences can be made about the physical state of a system that is not directly observable using measurement data provided by mobile radiation detection platforms? This chapter begins with a brief introduction to Bayesian methods of inference and a brief explanation of the Monte Carlo technique of particle filtering to approximate a distribution. The heart of this chapter focuses on the development the Bayesian model used by the Broad-Area Search Bayesian Processor (BASBP) and provides the mathematical framework for the estimates of the unknown state-space parameters.

3.1 Introduction to Bayesian Methods

A large body of work spanning 250 years documents the development of Bayesian methods and statistical decision theory. Most modern texts (such as those by Candy, Ghosh, and Robert [28]–[30]) on Bayesian methods begin with an introductory explanation of what makes Bayesian methods different from classical statistical approaches to data. The ability to infer information about the probability distribution from which a collection observations of random events occur serves a critical purpose in the field of statistical theory. Armed with an inferred probability distribution, one can either analyze past events and describe parameters of interest or one can offer some prediction regarding the parameters of future events as well as describe the uncertainties associated with the parameters in either case. However, the Bayesian's decision-oriented, interpretive view of the underlying distribution differs from the classical statistician's explanatory view. Whereas the Bayesian seeks an objective basis for choosing between competing hypothesis, the classical statistician explains the data in

terms of the underlying probability distribution. Well known examples of Bayesian methods include risk-reward scenarios such as gambling and investing in financial markets, electronic signal processing, target tracking, and wireless navigation.

Bayes' Rule serves the foundation of all Bayesian statistical methods. According to Bayes' Rule, the inference of properties regarding a set of unobserved random variables, $X_t = \{x(0), \cdots, x(t)\}$, based on a collection of data, $Y_t = \{y(0), \cdots, y(t)\}$, requires two essential components. Firstly, the likelihood $\pi(Y_t|X_t)$ that links the observed data (or evidence) to the unobserved variable. Secondly, the probability distribution that describes the observer's beliefs regarding the distribution of X_t before the data is collected, $\pi(X_t)$, known as the *prior* distribution. Equation 3.1 expresses Bayes' Rule as:

$$\pi(X_t|Y_t) = \frac{\pi(Y_t|X_t) \cdot \pi(X_t)}{\int_X \pi(X'_t)\pi(Y_t|X'_t)\mathrm{d}X'} = \frac{\pi(Y_t|X_t) \cdot \pi(X_t)}{\pi(Y_t)} \tag{3.1}$$

where $\pi(X_t|Y_t)$ is the joint posterior distribution, and the integration of the product of the likelihood and prior distributions over all possible values of X in the denominator yields probability distribution of the evidence. Under the conditions that the unobserved set of random variables, X_t is Markov (past, current, and future values of the sequence are independent) and the data at time t, $y(t)$, are conditionally independent of the past values of the unobserved variables, Bayes' rule can be expressed in sequential form as: [28], [29]

$$\pi(X_t|Y_t) = \frac{\pi(y(t)|x(t)) \cdot \pi(x(t)|x(t-1))}{\pi(y(t)|Y_{t-1})} \cdot \pi(X_{t-1}|Y_{t-1}) \tag{3.2}$$

From a computational perspective, the importance of Equation 3.2 stems from the fact that there is no need to carry the complete evolution of the data, likelihood and prior distributions. Only the current data and probability densities from the previous iteration in the sequence are required to calculate the posterior distribution. Unless the distributions are known exactly and the analytical solutions to the required integrations are available in closed form, the marginal posterior distribution (also known as the filtering distribution)

given in Equation 3.3 offers a more tractable solution:

$$\pi(x_t|Y_t) = \frac{\pi(y(t)|x(t)) \cdot \pi(x(t)|Y_{t-1})}{\pi(y(t)|Y_{t-1})} \tag{3.3}$$

Once the posterior distribution is known, a variety of Bayesian estimators can be calculated. The conditional mean (also known as the minimum mean-square error, MMSE) and the maximum *a posteriori* (MAP) estimator are the two most widely used estimators of the parameters of interest. The estimate of the conditional mean, $\hat{x}_{\text{MMSE}}$, is calculated by integrating the product of the dynamic variable and the posterior distribution as given in Equation 3.4:

$$\hat{x}_{\text{MMSE}} = E[x(t)|Y_t] = \int_X x(t)\pi(x(t)|Y_t)\mathrm{d}x \tag{3.4}$$

The MAP estimator, $\hat{x}_{\text{MAP}}$, is simply the most likely value of the dynamic variable given the posterior distribution:

$$\hat{x}_{\text{MAP}} = \underset{x(t)}{\operatorname{argmax}}\, \pi(x(t)|Y_t) \tag{3.5}$$

Along with the parameter estimators, estimates of the conditional variance can be computed, denoted as $R_{\text{x|y}}$, to express the uncertainty in the conditional mean using Equation 3.6 :

$$\begin{aligned} R_{\text{x|y}} &= E[(x(t) - E[x(t)|Y_t])^2|Y_t] \\ &= \int_X (x(t) - E[x(t)|Y_t])^2\pi(x(t)|Y_t)\mathrm{d}x \end{aligned} \tag{3.6}$$

Due to the interest in developing a Bayesian model that represents a complex and dynamic state of a system (not simply a statistical analysis of collected data), the next topic of focus is the general formulation of the Bayesian approach to state-space. From the previous discussion, and knowing that inferences made about the unobserved state of a system (state-space) using indirect observations (measurement space), requires a model that links the two

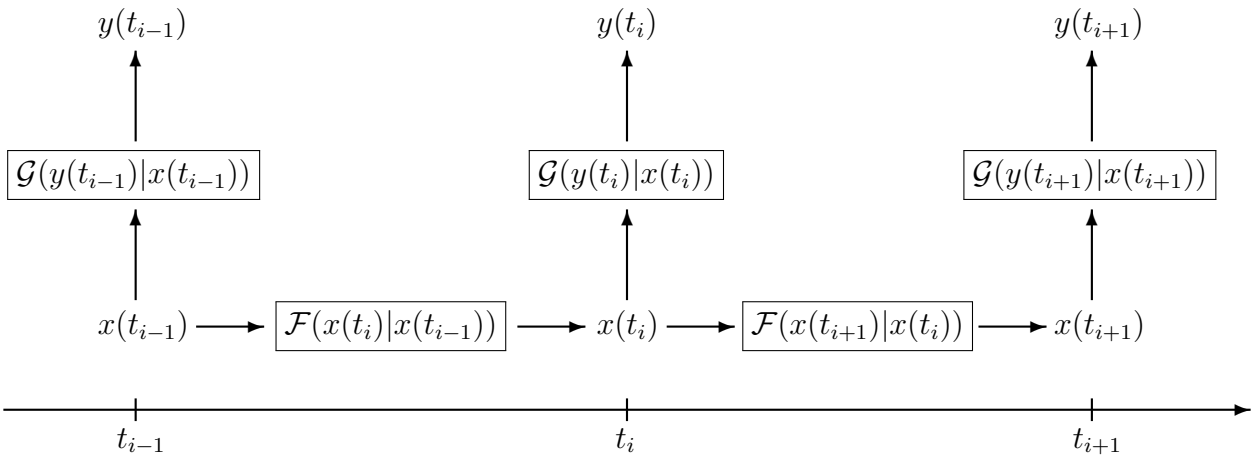

Figure 3.1: Evolution of the state- and measurement-spaces in time.

spaces. In its most basic form, Equation 3.7 provides the framework:

$$\begin{aligned} x_{t_i} &= \mathrm{F}(x_{t_{i-1}}, u_{t_{i-1}}, \omega_{t_{i-1}}) \quad \text{[State-space model]} \\ y_{t_i} &= \mathrm{G}(x_{t_i}, b_{t_i}, \nu_{t_i}) \qquad \text{[Measurement-space model]} \end{aligned} \tag{3.7}$$

where the $F(\cdot)$ and $G(\cdot)$ represent the state and measurement transition functions, respectively. The functions u_t and b_t represent known inputs to their respective transition functions. Process and measurement noise is reflected in the terms ω_t and ν_t. From J.V. Candy, it follows that both of the conditional probability distributions are completely specified by the functions $F(\cdot)$ and $G(\cdot)$ when combined with their respective noise distributions ($\pi(\omega)$ and $\pi(\nu)$).

$$\begin{aligned} \mathrm{F}(x_{t_{i-1}}, u_{t_{i-1}}, \omega_{t_{i-1}}) \Rightarrow \pi(x_{t_i}|x_{t_{i-1}}) \quad &\Leftrightarrow \mathcal{F}(x_{t_i}|x_{t_{i-1}}) \\ \mathrm{G}(x_{t_i}, b_{t_i}, \nu_{t_i}) \Rightarrow \pi(y_{t_i}|x_{t_i}) \quad &\Leftrightarrow \mathcal{G}(y_{t_i}|x_{t_i}) \end{aligned} \tag{3.8}$$

where $\mathcal{F}(x_{t_i}|x_{t_{i-1}})$ is the state transition probability and $\mathcal{G}(y_{t_i}|x_{t_i})$ is the conditional likelihood distribution. Figure 3.1 depicts the propagation of the state- and measurement-spaces in time.

3.2 Development of the Bayesian Model

Beginning the development of the BASBP model by defining the essential parameters, let the vector $\mathbf{x}_s$ represent the following characteristics of a radioactive source, s, of interest: the source's location in cartesian coordinates ($x_s(t), y_s(t), z_s(t)$ in meters), the source's velocity components in cartesian coordinates ($v_{x_s}(t), v_{y_s}(t)$, and $v_{z_s}(t)$ in meters per second), the strength of the source ($\mathcal{A}_s(t)$, in curies), the source's decay constant (λ_s, in seconds). As previously declared in section 2.6 sources of interest are assumed to be stationary and have half-lives much greater than the duration of the operational search. Based on these assumptions, the velocity components and the explicit time dependence of the state model can be dropped. Knowing that the data will be collected at discrete time intervals, let the index, k, maintain the sequence in time. The simplified vector, $\mathbf{x}_k^s$, of essential source parameters at time t_k is expressed as:

$$\mathbf{x}_k^s = [x_s, y_s, z_s, \mathcal{A}_s, \lambda_s]^\top, \tag{3.9}$$

where s is the source number ($s \in [1, \ldots, S]$), and $\top$ denotes the matrix transpose. The source parameter vectors for all the sources defining the state of the system can be collected into a stacked vector of S sources such that:

$$\mathbf{X}_k^S = [\mathbf{x}_1^\top, \ldots, \mathbf{x}_S^\top]^\top \tag{3.10}$$

Let the vector $\mathbf{y}_k$ represent the collection of measurements taken by radiation detection systems at time t_k within the operational search area. The minimum essential data collected by search platforms includes the following parameters: measurement duration (τ_k, in seconds), measurement location in cartesian coordinates (z_{x_k}, z_{y_k}, and z_{z_k}, in meters), and either counts recorded per energy bin ($y_k(E)$) or gross counts recorded (y_k), system dependent. Detection platforms may also include any number of other telemetry devices that collect information regarding the measurement environment at time τ_k and location $\mathbf{z}_k$.

Examples include visual, thermal, and hyper-spectral imaging sensors; as well as ambient temperature and humidity sensors.

The vector $\mathcal{D}_d$ defines characteristics of the detection platforms servicing the operational search, where $d = [1, \ldots, d_{\max}]$. Essential parameters of interest include: the detector's efficiency, ϵ_d; the area of the detector faces ($A_{1_{\mathrm{d}}}$ and $A_{2_{\mathrm{d}}}$, in centimeters^2) normal and perpendicular to the ground plane, respectively; and, the number and width of the energy bins used in the detector's output.

With the collection of essential parameters complete, the general form of the Bayesian state-space evolution model presented in Equation 3.7is revisited. Recalling that the radiation sources of interest are stationary, no physical processes alter the state parameters from one time interval to the next. Let the measurement function G be defined as a function of the following variables: the state-space, $\mathbf{X}_k^S$, the measurement location, $\mathbf{z}_k$, and the electronic measurement noise in detection system d, ν_{d_k}.

$$\mathbf{X}_k^S = \mathbf{X}_{k-1}^S \qquad \text{[State model]} \tag{3.11a}$$

$$y_k = \mathrm{G}(\mathbf{X}_k^S, \mathbf{z}_k, \nu_{\mathrm{d}_k}) \qquad \text{[Measurement model]} \tag{3.11b}$$

The corresponding conditional distributions are given by Equation 3.12 as:

$$\mathcal{F}(\mathbf{X}_k^S | \mathbf{X}_{k-1}^S) = 1 \tag{3.12a}$$

$$\mathcal{G}(y_k | \mathbf{X}_k^S) \propto \pi(y_k | \mathbf{X}_k^S) = \mathcal{P}\left(y_k | \Psi_k(\mathbf{X}_k^S, \mathbf{z}_k)\right) \tag{3.12b}$$

where $\Psi_k(\mathbf{X}_k^S, \mathbf{z}_k)$ is the expected radiation count at location $\mathbf{z}_k$. For brevity, the index k is dropped from the state-variable and denote it simply as $\mathbf{X}_S$. Expected radiation count, $\Psi_k(\mathbf{X}_S, \mathbf{z}_k)$, can be expand to account for the separate contributions from background sources and sources of interest, as well as the characteristic detector parameters and the measurement duration. The complete expression for the expected measurement is given by Equation 3.13:

$$\Psi_k(\mathbf{X}_S, \mathbf{z}_k) = \left(BG(\mathbf{z}_k) A_{1_{\mathrm{d}}} + \sum_{s=1}^{S} \phi_s^*(\mathbf{x}_s, \mathbf{z}_k) A_{\mathrm{d}}^*(\mathbf{x}_s, \mathbf{z}_k) \right) \cdot \epsilon_{\mathrm{d}} \cdot \tau_k \tag{3.13}$$

where $\mathrm{BG}(\mathbf{z}_k)$ is the expected photon flux at $\mathbf{z}_k$, $\phi_s^*(\mathbf{x}_s, \mathbf{z}_k)$ is the expected photon flux at $\mathbf{z}_k$ from the radiation source $\mathbf{x}_s$, and $A_{\mathrm{d}}^*(\mathbf{x}_s, \mathbf{z}_k)$ is the corrected area of a detector at $\mathbf{z}_k$ exposed to a radiation source located at $\mathbf{x}_s$. Equation 3.14 defines the areal correction in terms of the angle θ between the ground-facing, outward normal vector and the vector that points from the detector to the source.

$$A_{\mathrm{d}}^*(\mathbf{x}_s, \mathbf{z}_k) = A_{1_{\mathrm{d}}} \cos\left(\theta(\mathbf{x}_s, \mathbf{z}_k)\right) + A_{2_{\mathrm{d}}} \sin\left(\theta(\mathbf{x}_s, \mathbf{z}_k)\right) \tag{3.14}$$

This completes the essential elements of the Bayesian model used by the BASBP. The next section outlines Bayesian estimation procedures using the method of particle filtering.

3.3 Bayesian Estimation using Particle Filters

While a large variety of Bayesian signal filtering methods exist, the focus here is on the foundations of the Bayesian particle filtering methods used by the BASBP.* The bootstrap particle filter serves as a logical choice because the closed form of the measurement function, G, in Equation 3.11b does not exist. The only known connection between the measurement space and the state space is the conditional probability, $\mathcal{G}(y_k|\mathbf{X}_S)$, given in Equation 3.12b.

The Bayesian particle filter is a sequential Monte Carlo method of estimating the posterior distribution through sampling. In essence, discrete, random samples (called *particles*) are used to represent the continuous distribution of the unobserved state-space. Additionally, probability masses assigned to each particle represent the likelihood of the particle as the distribution evolves. Figure 3.2 depicts an example of a random set of 20 particles drawn from a given probability distribution.

As will be shown, the particles continuously evolve due to the recursive sampling from the updated transition distribution. Figure 3.4 depicts an example of the iterative propagation of the posterior distribution. Note that also shown is the track of the maximum *a posteriori* (MAP) estimate of the distribution (developed in the next section).

*Appendix B provides the basis for the Monte Carlo approximation of complex integrals. Here, only the essential components are reiterated in order to develop the mechanics needed for implementation in the BASBP.

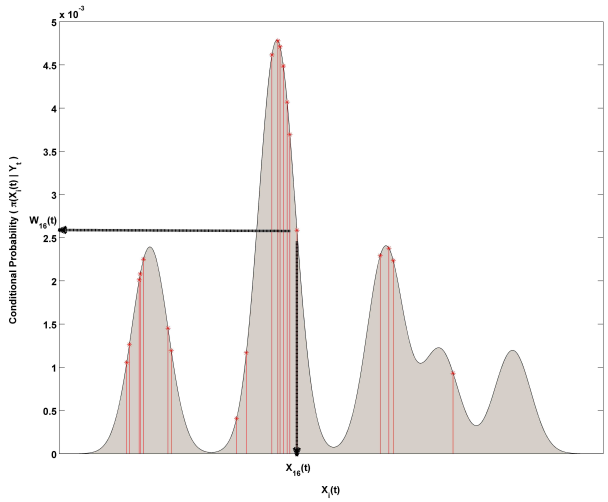

Figure 3.2: Sampling from the posterior distribution.

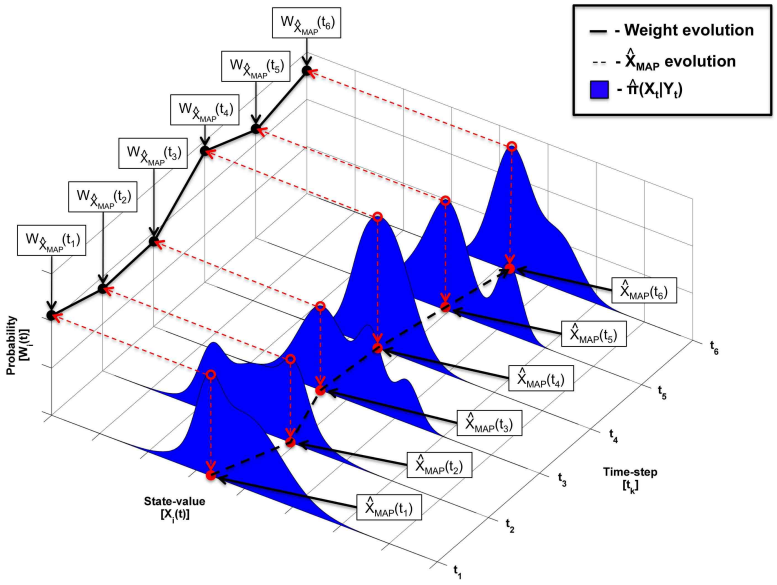

Figure 3.3: Particle propagation.

The generic particle filtering process begins by drawing N particles, $x_i(0)$, from the prior distribution and assigning a uniform weight,$w_i(0)$, to each particle. A new batch of particles, $x_i(t)$, is sampled from the state transition probability, $\mathcal{F}(x(t)|x_i(t-1))$, dictated by the state transition function F$(\cdot)$. Based on the foundation developed in Appendix B, it has been shown [28] that the weight given in Equation B.8 can be expanded in sequential

form, given in Equation 3.15 as:

$$w_t = w_{t-1} \cdot \frac{\pi(Y_t|X_t) \cdot \pi(X_t)}{\pi_q(X_t|Y_t)} = w_{t-1} \cdot \frac{\mathcal{G}(y_t|x_i(t)) \cdot \mathcal{F}(x(t)|x_i(t-1))}{\pi_q(x_i(t)|x_i(t-1), y(t))} \tag{3.15}$$

where π_q denotes the importance distribution. The particle weights receive an updated weight based on Equation 3.15 are then normalized. Given the updated particle weights the new estimate of the posterior distribution is obtained using Equation B.13 (repeated here for clarity):

$$\hat{\pi}(x_t|Y_t) \approx \sum_{i=1}^{N} w_i(t)\delta(x(t) - x_i(t)). \tag{3.16}$$

Table 3.1 outlines the algorithm for the generic Bayesian particle filter in concise form. While the general process is not complex, it should be noted that Bayesian particle filters suffer from the problem of degeneracy. That is, the variance of the importance weights, π_q, tends to increase with each iteration due to the sampling process. By preferentially selecting particles with higher weights, the algorithm degenerates to a single weight after a relatively few iterations [28]. One method of combating degeneracy is thru judicious selection of the the importance prior. The BASBP employs a form of the *bootstrap* particle filter [31] that uses the transition prior for the importance distribution as expressed in Equation 3.17:

$$\pi_q(x_i(t)|x_i(t-1), y(t)) \rightarrow \mathcal{F}(x(t)|x(t-1)) = 1 \tag{3.17}$$

where the definition of the transition distribution from the state-space model given in Equation 3.12a has been applied. The impact of selecting the transition prior as the importance distribution is two-fold: sampling the posterior distribution requires no additional computation; and, calculating the updated particle weights is greatly simplified. Using the transition prior reduces the weight update process:

$$w_t = w_{t-1} \cdot \mathcal{G}(y_t|x_i(t)) \tag{3.18}$$

While use of the transition prior simplifies the particle filtering process, note that it does not alleviate the problem of degeneracy.

Table 3.1: Algorithm for the Generalized Particle Filter

Method	Process
Initialization	
Draw: $x_i(0) \rightarrow \pi(x(0)), w_i(0) = 1/N,\ (i = 1, \ldots, N)$	[sample]
Importance Sampling	
Draw: $x_i(t) \sim \mathcal{F}(x(t)\|x_i(t-1))$	[state transition]
State-Space Transition	
$\mathcal{F}(x(t)\|x_i(t-1)) \Leftarrow F(x(t-1), u(t-1), \omega_i(t-1))$	
$\omega_i(t-1) \sim \pi(\omega_i(t))$	[transition]
Measurement Likelihood	
$\mathcal{G}(y(t)\|x_i(t)) \Leftarrow G(x(t), u(t), \nu(t)); \nu_i \sim \pi(\nu(t))$	[likelihood]
Weight Update	
$w_i(t) = w_i(t-1) \cdot \frac{\mathcal{G}(y(t)\|x_i(t)) \cdot \mathcal{F}(x(t)\|x_i(t-1))}{\pi_q(x_i(t)\|x_i(t-1), y(t))}$	[weights]
Weight Normalization	
$w_i(t) = w_i(t) / \sum_{i=1}^{N} w_i(t)$	[weight normalization]
Posterior Update	
$\hat{\pi}(x(t)\|Y_t) \approx \sum_{i=1}^{N} w_i(t)(x(t) - x_i(t))$	[posterior distribution]

A second technique often employed in particle filtering methods to combat particle degeneracy is known as resampling. Simply stated, the particle population is rejected and a new sample is drawn from the posterior distribution if the effective sample size falls below a designated threshold. It has been shown that the effective size of a population of particles can be characterized by the coefficient of variation [28]. The estimated effective sample size, $\hat{N}_{\text{eff}}$, is given in Equation 3.19 as:

$$\hat{N}_{\text{eff}} := \frac{1}{\sum_{i=1}^{N} w_i^2(t)} \tag{3.19}$$

Figure 3.4 depicts the process of resampling (the relative particle weights are denoted by their size). At the completion of the first iteration through the particle filter (the top row of particles in the graphic), the particles are evenly distributed in state-space, but their relative weights are proportional to the posterior distribution. Resampling from the importance sampling distribution discards particles with relatively low weights and replicates more particles from the higher-mass sections of the distribution. As the particles move through several cycles, their distribution converges on the unknown target distribution.

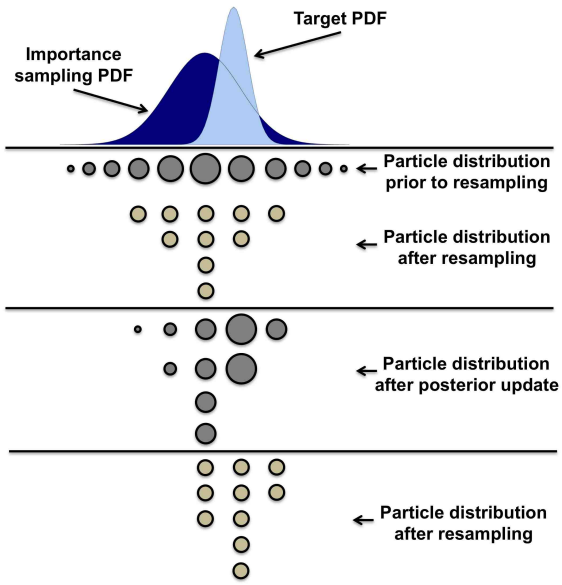

Figure 3.4: Notional depiction of the particle resampling method.

The third Bayesian technique used in the BASBP to prevent particle degeneracy is called *roughening*. In this method, artificial noise (or "jitter") is added to the particles via a random sample from the Normal distribution as given in Equation 3.20 [31], [32]:

$$\mathbf{x}_i^*(t) = \mathbf{x}_i(t) + \eta_i(t) \tag{3.20}$$

where $\mathbf{x}_i^*(t)$ denotes the *roughened* particle, and $\eta_i(t) \sim \mathcal{N}(0, J_k)$. J_k is a diagonal covariance matrix of size ($n_x \times n_x$, where n_x is the dimension size of $\mathbf{x}$). The elements of J_k are specified as: $\sigma_j^2 = (\kappa\ \mathcal{M}_n\ N^{-1/n_x})^2$. Here κ is a fixed, positive tuning parameter. $\mathcal{M}_n$ is maximum spread of the particle population in the n-th dimension, as given by:

$$\mathcal{M}_n = \max_{i,j} |x_i^{(n)} - x_j^{(n)}| \tag{3.21}$$

Scaling the standard deviation of the added noise by the inverse of the n_x-th root has the effect of normalizing the noise to the spacing on an equivalent rectangular grid of N points. Because the noise added to each particle stems from a continuous distribution, the process of *roughening* the particles has a similar effect to the more mathematically intensive procedure known as *regularization* [28], [33]. Namely, the roughening of particles keeps the processor from collapsing the distribution around a single point.

Roughening and regularization also has an impact on the sample size, N_p, required to adequately reflect the state-space. From the state-space model, the particles are stationary. This means that under sampling in the initial distribution can lead to erroneous posterior distributions if a radiation source exists in a region left void by the initial draw. Assuming the worst-case scenario, consider the case in which a uniform distribution is assigned to the spatial priors. If the search space covers 100 km^2, then 1E6 particles are required to represent the initial spatial domain as a uniform grid with a 10m grid-spacing. In addition to the spatial resolution, the BASBP requires: 6 stratifications to represent the possible number of sources; 10 stratifications to provide sufficient resolution of the source activity; and, another 10 stratifications to represent the 10 different potential sources of interest.

Without roughening, the problem posed would require 6.0E+9 particles. Use of roughening and regularization techniques provides the means for particles to drift into otherwise void regions and reduces the computational burden imposed by requiring enormous sample sizes.

Here, the generic particle filter algorithm is updated by incorporating the selection of the transition distribution for importance sampling and the use of resampling. As before, the bootstrap process begins by drawing N particles, $x_i(0)$, from the prior distribution and assigning a uniform weight,$w_i(0)$, to each particle. A new batch of particles, $x_i(t)$, is sampled from the state transition probability, $\mathcal{F}(x(t)|x_i(t-1))$, dictated by the state transition function $\mathrm{F}(\cdot)$. The particle weights receive their updated weight based on the product of their previous weight and the measurement likelihood. Following the weight updating step, the weights are normalized. After calculating the effective sample size, $\hat{N}_{\text{eff}}$, if the estimated effective size of the population exceeds a specified threshold, the algorithm proceeds as before. Otherwise, the particles are rejected and a new population is drawn by resampling from the importance distribution before proceeding with the posterior update. Table 3.2 outlines the generic bootstrap algorithm in mathematical form.

It is clear that the bootstrap particle filter offers a relatively simple way of approaching analytically intractable problems. In the next section, the Bayesian estimation of parameters introduced previously is revisited in order to further outline the Monte Carlo-based approach using particle filters.

Table 3.2: Algorithm for the General Bootstrap Particle Filter

Method	Process
Initialization	
Draw: $x_i(0) \rightarrow \pi(x(0)), w_i(0) = 1/N,\ (i = 1, \ldots, N)$	[sample]
Importance Sampling	
Draw: $x_i(t) \sim \mathcal{F}(x(t)\|x_i(t-1)) \Leftarrow F(x(t-1), u(t-1), \omega_i(t-1))$ $\omega_i(t-1) \sim \pi(\omega_i(t))$	[state transition]
Weight Update	
$w_i(t) = w_i(t-1) \cdot \mathcal{G}(y(t)\|x_i(t)) \Leftarrow G(x(t), u(t), \nu(t); \nu_i \sim \pi(\nu(t))$	[weights]
Weight Normalization	
$w_i(t) = w_i(t) / \sum_{i=1}^{N} w_i(t)$	[weight normalization]
Resampling Decision	
$\hat{N}_{\text{eff}} = 1 / \sum_{i=1}^{N} w_i^2(t);\ \hat{N}_{\text{eff}} \leq N_{\text{threshold}} \rightarrow$ Resample	[effective samples]
Resampling	
$\hat{x}_i(t) \Rightarrow x_i(t)$	[resample]
Roughening	
$\hat{x}_i(t) \Rightarrow x_i(t) + \eta_i(t)$	[roughening]
Posterior Update	
$\hat{\pi}(x(t)\|Y_t) \approx \sum_{i=1}^{N} w_i(t)(x(t) - x_i(t))$	[posterior distribution]

3.4 Obtaining Parameter Estimates from Particle Filters

Briefly returning to the Bayesian parameter estimation, this section defines the methods for calculating the required parameter estimates based on the BASBP's use of Monte Carlo particle filtering methods. As previously described, particle filtering methods provide a means to approximate problematic integrations. This process begins with the output of the *posterior* update process. That is, the current set of Monte Carlo particles and their associated weights, $[x_i, w_i]_{i=1}^{N}$ are known as well as the estimate of the posterior distribution, $\hat{\pi}(X_(t)|Y_t)$, as given by:

$$\hat{\pi}(X_t|Y_t) \approx \sum_{i=1}^{N} w_i(t)\delta(X_t - x_i(t)). \tag{3.22}$$

The MMSE parameter estimate, $\hat{x}_{\text{MMSE}}$, from Equation 3.4 is estimated by applying the Monte Carlo principles outlined in Appendix B combined with the current estimate of posterior distribution, $\hat{\pi}(X_t|Y_t)$:

$$\begin{aligned}
\hat{x}_{\text{MMSE}} = E_{\hat{\pi}}[x(t)|Y_t] &= \int_X x(t)\hat{\pi}(X_t|Y_t)\mathrm{d}x \\
&= \int_X x(t)\hat{\pi}(X_t|Y_t)\mathrm{d}x \\
&= \int_X \sum_{i=1}^{N_p} x_i(t)w_i(t)\delta(x(t) - x_i(t)) = \sum_{i=1}^{N_p} w_i(t)x_i(t)
\end{aligned} \tag{3.23}$$

The MAP estimator only requires the simple replacement of the posterior distribution with the current estimate of the posterior, $\hat{\pi}(X_t|Y_t)$:

$$\begin{aligned}
\hat{x}_{\text{MAP}} &= \underset{x(t)}{\operatorname{argmax}}\, \pi(X(t)|Y_t) \\
&\approx \underset{x_i(t)}{\operatorname{argmax}}\, \hat{\pi}(x(t)|Y_t)
\end{aligned} \tag{3.24}$$

Where the estimation of the variance of the conditional, $R_{\mathrm{x|y}}$, is given by:

$$\begin{aligned} R_{\mathrm{x|y}} &= E\left[(x(t) - E[x(t)|Y_t])^2|Y_t\right] \\ &= \int_X (x(t) - E[x(t)|Y_t])^2 \, \pi(X_t|Y_t)\mathrm{d}x \end{aligned} \tag{3.25}$$

using Monte Carlo-based importance sampling, the conditional variance can be estimated by sampling from the posterior distribution and employing the estimate of the conditional mean, $\hat{x}_{\mathrm{MMSE}}$, in Equation 3.26:

$$\begin{aligned} \hat{R}_{\mathrm{x|y}} &= \int_X (x(t) - E[x(t)|Y_t])^2 \hat{\pi}(x(t)|Y_t)\mathrm{d}x \\ &= \sum_{i=1}^{N_p} w_i(t)\delta(x(t) - x_i(t))(x(t) - \hat{x}_{\mathrm{MMSE}})^2 \\ &= \sum_{i=1}^{N_p} w_i(t)(x_i(t) - \hat{x}_{\mathrm{MMSE}})^2 \end{aligned} \tag{3.26}$$

To conclude the discussion of the basic Bayesian principles and the particle filtering process, note that two central factors are expected to affect implementation of these methods in the Bayesian processor:

- The selection of the prior distributions embedded in $\pi(\mathbf{x})$;
- The splitting of the measured signal into the components of $\Psi_k(\mathbf{X}_S, \mathbf{z}_k)$; and
- The execution of the detection decision inherent in the measurement likelihood function, $\mathcal{G}$;

With these issue items at the fore, the next chapter outlines of the development of the BASBP.

4 | Development of the Bayesian Processor

This chapter develops the Broad-Area Search Bayesian Processor (BASBP) based on the foundation of Bayesian methods and radiation detection principles established in Chapter 3. The primary functions of the processor include: process knowledge of the broad-area search problem and establish the source parameter *prior* distributions; receive and process radiation detection system data; estimate the local background radiation; determine whether or not the observed measurement includes a source signal; estimate the *posterior* distribution of the source parameters; provide updated estimates of the source parameters of interest; and provide updated guidance to the sensor platforms. With these core tasks in mind, Figure 4.1 depicts the flow of information within the BASBP and serves as the roadmap followed in the development of the processor in this chapter.

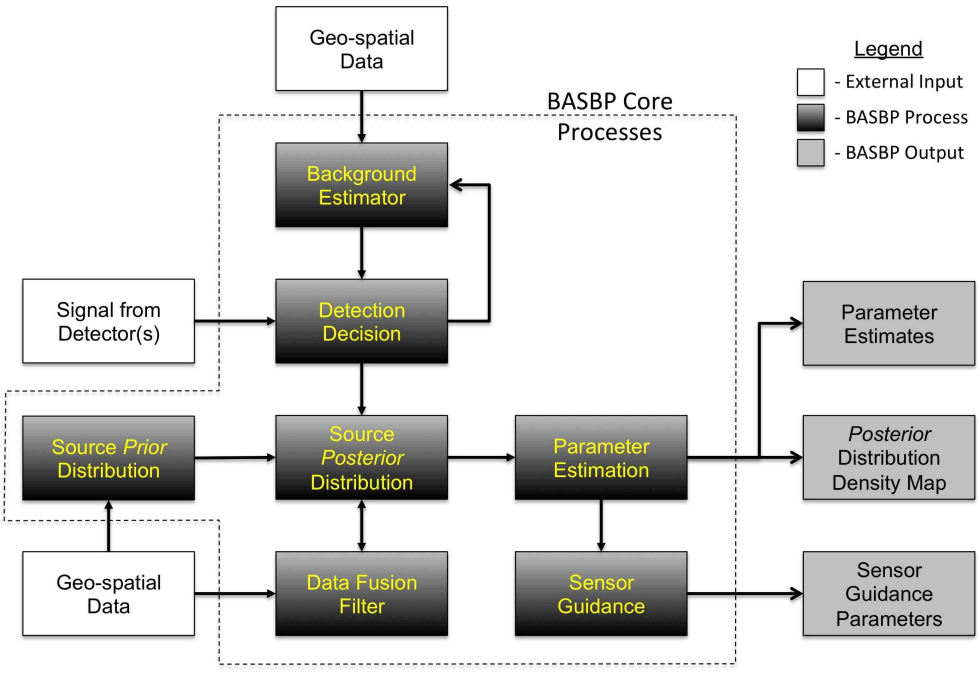

Figure 4.1: Flowchart of BASBP processes.

4.1 Selection of *Priors* for the Source Particle Filter

The primary source parameters of interest include the number of radioactive sources in the search space and their location, intensity, and type. The selection of *priors* revolves entirely around knowledge of the broad-area search problem (including how the problem originated) and the environmental factors influencing the search space. Prior knowledge informs the beliefs regarding the distribution of the parameters of interest. Where prior beliefs offer little information regarding the distribution of a parameter, the uninformative uniform distribution must be chosen. In most cases, however, the ability to leverage knowledge of the problem and environment to construct credible parameter distributions will prevent having to default to the uniform distribution. Examples of the types of information useful in the construction of BASBP *priors* include:

- Information related to the events triggering the broad-area search problem:
  - cause for the search (sensors triggered; lost, missing, or stolen sources; or, radiation sickness reported by the general population);
  - source number, type, and intensity; and,
  - knowledge of potential suspects, their motivations, and intentions.
- Geo-spatial data concerning the search space:
  - census and demographic data;
  - topography data;
  - visual, thermal, or hyper-spectral imagery;
  - radiological survey data; and,
  - weather data

In the implementation of the bootstrap particle filter used to estimate the source parameters in the BASBP, the state-space is represented by N Monte Carlo particles, $\mathbf{X} \in \mathbb{R}^{N \times 5 \times r_{\max}}$. Each particle represents a number of sources, r, where $r \in [0, r_{\max}]$, and r is drawn from the *prior* distribution π_r. The values of the number of sources represented by each particle is stored in a vector, $\mathbf{r}$ (where $\mathbf{r} \in \mathbb{R}^N$). Recall that each source contains the 5 parameters of

Table 4.1: Initial Particle Sampling Algorithm

Line	Process
1 :	**Subroutine** Draw Particles $(N, [\mathbf{X}_0^n, \mathbf{r}_0^n, \mathbf{w}_0^n]_{n=1}^N)$
2 :	**Do** $i = 1, N$
3 :	Sample $r_i \sim \pi_r$
4 :	**Do** $j = 1, \max(1, r_i)$
5 :	Sample $\mathbf{x}_0^{i,j} \sim \pi_{xy}$
6 :	Sample $\mathcal{A}_0^{i,j} \sim \pi_{\mathcal{A}}$
7 :	Sample $\lambda_0^{i,j} \sim \pi_{\lambda}$
8 :	**End Do**
9 :	**End Do**
10 :	Set $[\mathbf{w}_0^n = 1/N]_{n=1}^N$
11 :	**End Subroutine** Draw Particles

interest as defined in Section 3.2, where $\mathbf{x_s} = [x_s, y_s, z_s, \mathcal{A}_s, \lambda_s]$. Table 4.1 lists the general process used to generate the initial set of source particles. The next few subsections describe how the *priors* are selected for each of the four sampling procedures.

4.1.1 *Priors* for the Distribution of the Expected Number of Sources

If no information exists to define the relative likelihoods across the range of possible source numbers, r, then the logical choice for the *prior*, π_r is the Uniform distribution, where $r \sim \mathcal{U}(0, r_{\max})$. Ristic (et al) suggest using the linearly decreasing, discrete function given by Equation 4.1 to define π_r [10]. Figure 4.2 depicts the distribution of π_r as a function of the number of sources.

$$\pi(r) = \frac{r_{\max} - r + 1}{\sum_{r=0}^{r_{\max}} r + 1} \tag{4.1}$$

Clearly, this distribution places more emphasis on the lower range of possible sources as opposed to the upper range. Reducing the sampling weights of less likely components of π_r conserves Monte Carlo particles and reduces computation time.

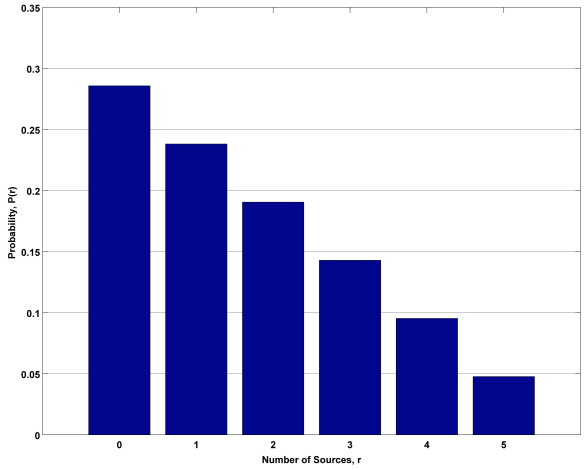

Figure 4.2: Example probability distribution of the number of sources.

4.1.2 *Priors* for the Distribution of Sources in the Spatial Domain

The spatial distributions of the unknown source parameters x_s, y_s, and z_s are constrained by the critical assumptions listed in Table 2.1. Due to the assumption that radioactive sources are confined to the surface of the ground, the focus here is on estimating how the sources are distributed in the x-, and y-dimensions (easting and northing), π_x, π_y. Once a particles coordinates have been chosen, the elevation of the particle is set to ground level at that location.* At the time of initiation of the broad-area search problem, selection of the Uniform distribution, $\mathcal{U}(\min, \max)$, offers a rapidly implementable choice for each dimension. However, the use of a non-informative *prior* should be reserved for cases in which no information exists to refine the spatial bounds of the problem.

A broad range of information may be available to law enforcement and government entities capable of narrowing the dimensions of the broad-area search space. However, the discussion herein focuses on demonstrating the development of *priors* for the distribution of spatial source parameters based solely on the analysis of geographic data sets typically available to the public. Common datasets include: standard maps, land-use data from satellite scans, elevation data, and imagery data. As a generic example, likelihood values

*Alternatively, when radar telemetry is available, the elevation of each particle can be set to zero and the measurement elevation can be set to the detector's height above ground.

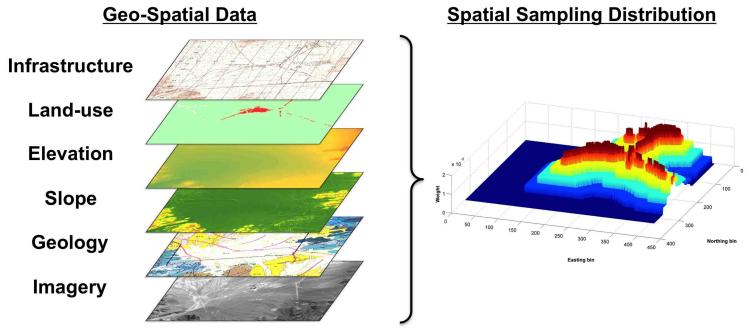

Figure 4.3: Aggregation of spatial data to create spatial weighting distribution.

assigned to the pixels in a land-cover scene can signify beliefs that a source is more likely to be found in an urban environment vice wetlands or a body of water. Similarly, circumstances may allow for the exclusion of steep terrain as identified by analyzing surface elevation data. After assigning likelihood values to the pixels in a geo-spatially coded scene, normalizing the values results in a relative weighting map suitable for sampling the pixels, π_{xy}. Figure 4.3 depicts the aggregation of geo-spatial data to develop a spatial importance sampling distribution. The spatial sampling resolution, however, depends on the resolution of the geo-spatial data used to generate the pixel weighting map.[†] Within each pixel, it is assumed that the spatial distribution is uniform and random samples are drawn for the easting and northing coordinate.

Note that in order to facilitate computations using SI units, portions of the National Geospatial-Intelligence Agency's publicly available source code for the geographic translator, GEOTRANS [34], were translated into FORTAN to rapidly translate locations given in units of decimal degrees to meters using the Universal Transverse Mercator (UTM) format. The incorporation of a highly accurate, stand-alone translation service provides the BASBP the ability to rapidly translate coordinates (in either direction), either as a single coordinate conversion or in bulk.

[†]Typical, publicly available, geo-spatial data sets based on satellite sensors have resolutions on the order of 1 arc second, or approximately 25 meters.

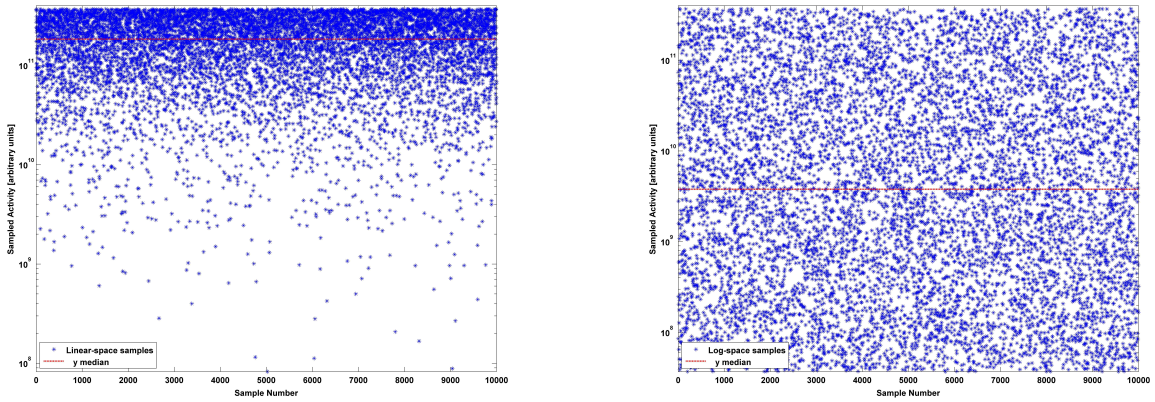

(a) Sampling in linear space. **(b) Sampling in log-space.**

Figure 4.4: Results of random source activity sampling using the Uniform distribution.

4.1.3 *Priors* for the Source Strength

Radiation source strength, $\mathcal{A}_s$, is typically measured in terms of source activity – the mean number of decays occurring per second. As with previous *priors*, if little information exists regarding the distribution of the source strength, then one must default to the Uniform distribution, $\pi_{\mathcal{A}} \sim \mathcal{U}(\mathcal{A}_{\min}, \mathcal{A}_{\max})$. If the difference between the lower and upper bounds of the source strength is greater than a decade, however, Equation 4.2 must be used in order to draw random samples from $\pi_{\mathcal{A}}$ uniformly.

$$\mathcal{A}_i = 10^{\left[\log(\mathcal{A}_{\min}) + \chi_i \cdot \log(\frac{\mathcal{A}_{\max}}{\mathcal{A}_{\min}})\right]} \tag{4.2}$$

where χ_i is a random variate drawn $\sim \mathcal{U}(0, 1)$. Figure 4.4 depicts the results after drawing 10,000 samples using Equation 4.2 and $\mathcal{A} \in [0.001, 10.000]$ in curies. As shown in Figure 4.4a, improper sampling occurs if samples are drawn linearly from an exponential range of activities. On the other hand, when reason exists to believe that the source strength falls within a narrow range, a much tighter distribution (like the Gamma distribution, with appropriate shape and scale parameters) may be more appropriate.

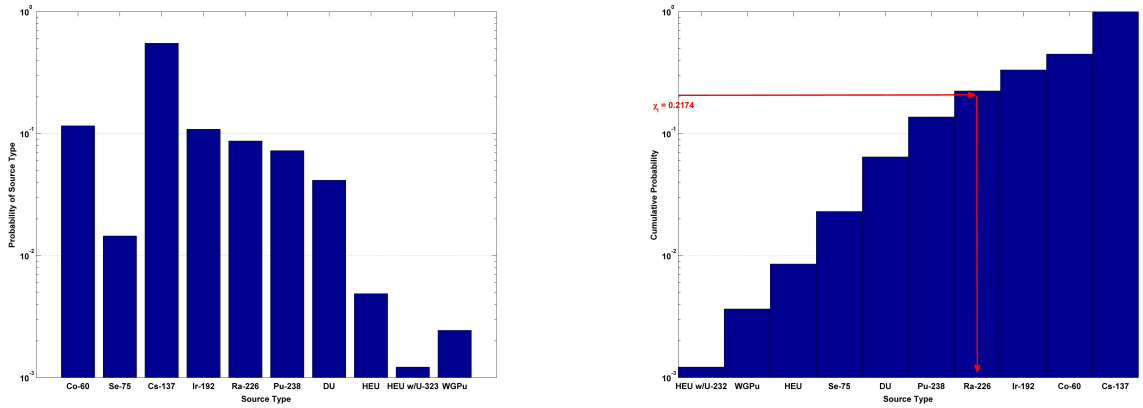

(a) Probability distribution. **(b) Cumulative probability distribution.**

Figure 4.5: Sampling from the source type probability distribution, π_λ.

4.1.4 *Priors* for the Source Type Distribution

The selection of the source type distribution, π_λ, revolves around the information available regarding the events that triggered the broad-area search. The Uniform distribution represents the case where the analysis of available information fails to narrow the list of possible source types. For uniformly likely source types, the probability of sampling any one source is equal to $1/N_\lambda$, where N_λ is the number of possible source types. However, information may exclude or significantly reduce the likelihood of finding specific source types. The discrete distribution for π_λ is constructed by weighting each source type according to the beliefs in the relative likelihood of occurrence and then normalizing the weight distribution. Recalling the data from the IAEA's ITDB depicted in Figure 2.2, a discrete likelihood distribution can be generated by applying the additional assumption that SNM sources are 100-times less likely than conventional radiation sources. Figure 4.5a depicts the resulting source-type distribution. Figure 4.5b the sampling from π_λ using an inverse transformation by a uniformly drawn sample in the interval $[0, 1]$, denoted as χ_i, from the cumulative distribution function of π_λ and mapping it to the corresponding discrete source type.

Having established the framework for estimating the *priors* for the source parameters and drawing the initial samples, the next section proceeds with the development of the BASBP

framework by focusing attention on the process by which the local background parameters are estimated.

4.2 Background Estimation

4.2.1 *Priors* for the Local Background

It is well known fact that three distinct sources of background gamma radiation exist: cosmic sources; reactions in the atmosphere with cosmic radiation; and terrestrial, naturally occurring radioactive materials (NORM). Terrestrial background radiation varies spatially due to variations in geology, terrain, and the construction materials used in man-made objects. Altitude and distance from the surface of the earth also impact the magnitude and energy distribution of the gamma radiation attributable to background sources. The magnitude and spectral content of the local background radiation varies temporally as well. Neglecting the obvious change in local background environments due to man-made construction or demolition projects, the most significant time-based variations in background radiation stem from changes in the solar radiation due to the earth's rotation and the weather. [35]

Assuming that one can estimate the magnitude of the background radiation signal due to NORM based on a previous measurement, one can also apply a correction factor to adjust both the cosmic radiation and the temporal effects of the local weather.

The BASBP assumes that variations in the background radiation due to NORM are consistent with spatial variations in the land-cover categories. In the BASBP, two operational approaches to estimating the *prior* distribution, π_{BG}, of the local background flux based on geo-spatial land-cover data are considered:

- **Use of training data.** Time and terrain permitting, develop a training database of background measurements based on similar terrain types to those found within the search space.

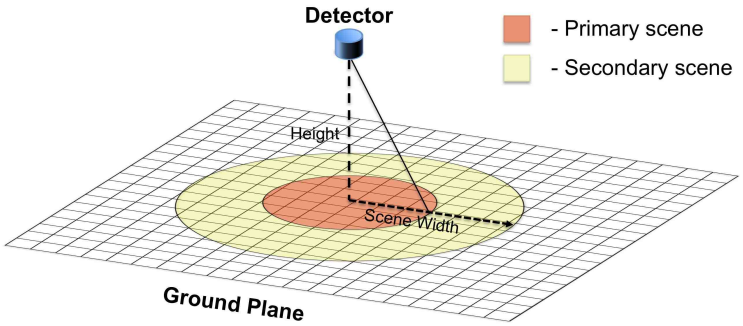

Figure 4.6: Geometry influencing scene-size selection.

- **Use of correlation matrix.** Develop a correlation matrix that describes the gradient when moving between terrain types.

The scene size and content serve as the critical factors impacting the ability to base the background estimate off of terrain type. The size of the scene is defined based on the height of the detector above the surface of the ground as the width of the scene in land-cover pixels. The *primary scene* consists of those land-cover pixels nearest the detector while the *secondary scene* consists of those pixels on the margins of the detector's field of view. Figure 4.6 depicts the relationship between the detector and the scene selection on the ground plane. Based on the 16 land-cover categories used in the land-cover products available from the U.S. Army Geospatial Center [36], let the vector $\boldsymbol{\Xi}_j$ as defined in Equation 4.3 to represent the land-cover scene within the detector's FOV at z_k:

$$\boldsymbol{\Xi}_j = [P_{\xi_1}, \cdots, P_{\xi_{16}}, S_{\xi_1}, \cdots, S_{\xi_{16}}] \tag{4.3}$$

where j corresponds to the index of the row in Ξ that matches the land-cover scene at z_k, $[P_{\xi_i}]_{i=1}^{16}$ is a vector consisting of the number of pixels in the primary scene of each land-cover type, ξ_i ($\xi_i \in [0, 1, \ldots, 15]$), and $[S_{\xi_i}]_{i=1}^{16}$ contains the corresponding information for the secondary scene.

4.2.2 Development of the Bootstrap Particle Filter for the Background Estimates

In addition to the estimate of the posterior distribution, the BASBP utilizes a bootstrap particle filter to estimate the background flux, $\widehat{\mathbf{BG}}_j$, predicted for the land-cover scene Ξ_j at the detector location, z_k. The background estimation problem can be stated as: given a set of noisy gamma-ray measurements, $\{\mathrm{BG}_{\mathrm{obs}}^k\}$, and a set of *prior* parameters, $\{\mathrm{BG}_0, w_0\}$, determine the best estimates of the background flux, $\widehat{\mathrm{BG}}$, and the standard error of the background flux estimate, $\widehat{\mathrm{BG}}_{\mathrm{RMSE}}$. Equation 4.4 establishes the relationship between the State-space and Measurement-space needed for the particle filter.

$$\begin{aligned} \mathrm{BG}_m &= \mathrm{BG}_{m-1} + w_{m-1} \quad \text{[State-space]} \\ \mathrm{BG}_{\mathrm{obs}}^m &= \mathcal{C} \cdot \mathrm{BG}_m + \nu_m \quad \text{[Measurement-space]} \\ \mathcal{C} &= \epsilon_{\mathrm{det}} \mathcal{A}_{\mathrm{det}} \tau \end{aligned} \tag{4.4}$$

where m is the m-th observation of the land-cover scene Ξ_j, w_{m-1} is the process noise (due to radioactive decay and radiation transport processes) associated with the background flux ($w_{m-1} \sim \mathcal{N}(0, \mathrm{BG}_{m-1})$), ν_m is the systematic measurement noise ($\nu_m \sim \mathcal{N}(0, \sigma_\nu^2)$), and $\mathcal{C}$ is a scaling factor based on detector properties (efficiency and area) and the measurement time, τ.

In the implementation of the BASBP, measurement noise is neglected due to the assumption that $\mathrm{BG}_{m-1} \gg \sigma_\nu^2$. The detection decision function (see Section 4.3) determines that portion of the observed signal, y_k, attributable to the local background, $\mathrm{BG}_{\mathrm{obs}}^m$. Further, let the concatenated vector $\widehat{\mathbf{BG}}_j$ store the key background particle filter variables, as defined by Equation 4.5:

$$\widehat{\mathbf{BG}}_j = [\mathbf{BG}, \mathbf{w}, \widehat{\mathrm{BG}}, \widehat{\mathrm{BG}}_{\mathrm{RMSE}}] \tag{4.5}$$

where $\mathbf{BG}_j$ is the set of N_{BG} Monte Carlo particles representing the estimated average background flux for scene Ξ_j, $\mathbf{w}$ is the vector of particle weights, $\widehat{\mathrm{BG}}$ is latest background estimate, and $\widehat{\mathrm{BG}}_{\mathrm{RMSE}}$ is the standard deviation of the estimate. Table 4.2 outlines the procedures used to implement the background estimator.

Table 4.2: Algorithm for Background Estimate Particle Filter

Line	Process
1 :	**Subroutine** Background Particle Filter $(\widehat{\mathbf{BG}}_j^{m-1}, \mathrm{BG}_{\mathrm{obs}}^k)$
2 :	Update weights: $w_i^m = w_i^{m-1} \cdot \mathbb{P}(\mathrm{BG}_{\mathrm{obs}}^k \vert \mathrm{BG}_i, \sqrt{\mathrm{BG}_i})$
3 :	Normalize weights: $w_i^m = w_i^m / \sum_{i=1}^{N_{\mathrm{BG}}} w_i^m$
4 :	Calculate $N_{\mathrm{eff}} = 1/\sum_{i=1}^{N_{\mathrm{BG}}} (w_i^m)^2$
5 :	**If** $N_{\mathrm{eff}} \leq N_{threshold}$ **then**
6 :	$[\mathbf{BG}^m, \mathbf{w}^m] =$ **Resample** $[\mathbf{BG}^m, \mathbf{w}^m]$.
7 :	**End If**
8 :	Update estimates: $\widehat{\mathrm{BG}}, \widehat{\mathrm{BG}}_{\mathrm{RMSE}}$
9 :	**End Subroutine** Background Particle Filter

4.3 The Detection Decision

The radiation detection decision facing the BASBP is cast in terms of two competing hypotheses. The null hypothesis addresses the state in which no source signal exists and the observed measurement stems solely from the local background signal and measurement noise. The alternative hypothesis addresses the state in which the measured signal is the sum of the background and source signal arriving at the detector at the same time, combined with measurement noise. Equation 4.6 expresses the two hypotheses in mathematical form:

$$\begin{aligned} \mathcal{H}_0 &: y_k(\mathbf{z}_k) = \mathcal{R}\left(\overline{\mathrm{BG}}(\mathbf{z}_k)\right) + \nu(k) && \text{[No-source present]} \\ \mathcal{H}_1 &: y_k(\mathbf{z}_k) = \mathcal{R}\left(\overline{\mathrm{BG}}(\mathbf{z}_k), \bar{S}(\mathbf{z}_k)\right) + \nu(k) && \text{[Source present]} \end{aligned} \tag{4.6}$$

where $\mathcal{R}\left(\overline{\mathrm{BG}}(\mathbf{z}_k)\right)$ under $\mathcal{H}_0$ is a realization of a random sample from the Poisson distribution with a mean count rate of $\overline{\mathrm{BG}}$ located at $\mathbf{z}_k$, and $\nu(k)$ is the zero-mean, Gaussian measurement noise ($\nu \sim \mathcal{N}(0, \sigma_\nu^2)$). Under $\mathcal{H}_1$, $\mathcal{R}$ depends upon both the $\overline{\mathrm{BG}}(\mathbf{z}_k)$ and the contribution at $\mathbf{z}_k$ due to the presence of a radiation source, also drawn from the Poisson distribution, with a mean count rate of $\bar{S}(\mathbf{z}_k)$. Because $\overline{\mathrm{BG}}$ varies with measurement location, a sequential hypothesis test similar to the one employed by Candy (et al) to drive the alarm

decision for a stationary portal monitoring system cannot be employed [7]. Instead, the BASBP uses the following likelihood ratio statistic: [29]

$$\Lambda = \frac{\sup_{\theta \in \Theta_1} f(x|\theta)}{f(x|\theta_0)} \tag{4.7}$$

where $f(x|\theta)$ is the likelihood function for the random variable x with parameter θ, θ_0 is the value of theta under the null hypothesis, and Θ_1 is the set of all values of θ for which the alternate hypothesis is true. Expressing Equation 4.7 in terms of the detection decision:

$$\Lambda[y_k] = \frac{\sup \mathbb{P}(\mathcal{R}, \mathcal{H}_1)}{\mathbb{P}(\mathcal{R}, \mathcal{H}_0)} = \frac{\underset{i \in [1,\ldots,\widehat{\mathrm{BG}}(\mathbf{z}_k)]}{\operatorname{argmax}} \left[\mathcal{P}\left((y_k - i | \widehat{\mathrm{BG}}(\mathbf{z}_k) \right) \cdot \mathcal{P}(i|i) \right]}{\mathcal{P}\left((y_k | \widehat{\mathrm{BG}}(\mathbf{z}_k) \right) \cdot \mathcal{P}(0|1)} \tag{4.8}$$

where under $\mathcal{H}_1$, all combinations of background and source contributions capable of giving rise to the observed measurement are considered. Of note, the Poisson probability $\mathcal{P}(0|1)$ is used in the denominator to estimate the probability of not having a source signal present as opposed using $\mathcal{P}(0|0)$. The rationale is straight forward: using $\mathcal{P}(0|0) = 1$, the decision function will always choose the null hypothesis. Using $\mathcal{P}(0|1)$ when $\mathcal{P}(0|1) = \mathcal{P}(1|1)$, negates only the detection decision when the source contribution is identically equal to 1 — which is well below the decision threshold.

The threshold for deciding between $\mathcal{H}_0$ and $\mathcal{H}_1$ is established according to the probabilities of committing errors of the first and second kinds. An error of the first kind occurs when the null hypothesis is rejected when in fact true (false positive, FP). An error of the second kind occurs when the null hypothesis is accepted when false (false negative, FN). It is common practice to characterize radiation detection systems with their associated receiver-operating curves (also known as ROC curves) which depict the interaction between the probabilities of a FP and FN alarm occurring (P_{FP} and P_{FN}, respectively) based on an established decision threshold. Based on the detection threshold established for the radiation detection system and corresponding P_{FP} and P_{FN} values, the threshold for the BASBP detection decision is

Table 4.3: Detection Decision Algorithm

Line	Process
1 :	**Function** Detection Decision $(y_k, \widehat{BG}_k, \mathbb{P}_{\text{FP}}, \mathbb{P}_{\text{FN}})$
2 :	**If** $y_k > \widehat{BG}_k$ **then**
3 :	Set $\mathcal{T}_{det} = \frac{1-\text{P}_{\text{FN}}}{\text{P}_{\text{FP}}}$ and $N = y_k - \widehat{BG}_k$.
4 :	Let $[\text{BG}^i_{\text{est}} = y_k - i, \text{Sig}^i_{\text{est}} = i]^N_{i=0}$.
5 :	Let $\mathbb{P}^0 = \mathcal{P}(\text{BG}^0_{\text{est}}\|\widehat{BG}_k) \cdot \mathcal{P}(0\|1)$.
6 :	Let $[\mathbb{P}^i = \mathcal{P}(\text{BG}^i_{\text{est}}\|\widehat{BG}_k) \cdot \mathcal{P}(\text{Sig}^i_{\text{est}}\|\text{S}^i_{\text{est}})]^N_{i=1}$.
7 :	Let $\Lambda_k = \underset{i\in[1,\ldots,\widehat{\text{BG}}(\mathbf{z}_k)]}{\text{argmax}} \mathbb{P}^i/\mathbb{P}^0$.
8 :	**If** $\Lambda_k \geq \mathcal{T}_{\text{det}}$ **then** let $\text{BG}_{est}(\mathbf{z}_k) = \text{BG}^i_{\text{est}}, \text{Sig}_{\text{est}}(\mathbf{z}_k) = \text{Sig}^i_{\text{est}}$
9 :	**Else** let $\text{BG}_{est}(\mathbf{z}_k) = y_k, \text{Sig}_{\text{est}}(\mathbf{z}_k) = 0$ **End If**.
10 :	**End If**
11 :	**End Function** Detection Decision

calculated as:

$$\mathcal{T}_{\text{det}} = \frac{1 - \text{P}_{\text{FN}}}{\text{P}_{\text{FP}}} \tag{4.9}$$

where the numerator is also known as the power of detecting $\mathcal{H}_1$. Given the decision threshold $\mathcal{T}_{\text{det}}$, the null hypothesis is rejected (no source signal is present) only when the decision function Λ exceeds the specified threshold, as expressed in Equation 4.10:

$$\begin{aligned} \Lambda_k &\geq \mathcal{T} \quad \text{Accept } \mathcal{H}_1 \\ \Lambda_k &< \mathcal{T} \quad \text{Accept } \mathcal{H}_0 \end{aligned} \tag{4.10}$$

If the Λ_k decision function points towards accepting $\mathcal{H}_0$, then the current measurement value y_k is assigned to the background estimate for the measurement location, $\text{BG}_{est}(\mathbf{z}_k)$, and the estimate of the source signal, $\text{Sig}_{\text{est}}(\mathbf{z}_k)$, is set to zero. Otherwise, the background estimate is assigned the value of $y_k - i$ and the source signal is set to the value of i, both from Equation 4.8. Table 4.3 lists the algorithm for implementing the detection decision function in the BASBP. With the local background and source signal estimations in hand, development of the BASBP proceeds with the estimation of the updated posterior distribution.

4.4 The Posterior Distribution Update

The process of updating the posterior distribution serves as the workhorse of Bayesian particle filtering methods. While the concept of updating the posterior distribution from the general bootstrap particle filter algorithm given in Section 3.3 is straight forward, the nature of the broad-area search problem dictates a unique approach to implementing the processes involved. In particular, the BASBP employs the following unique features: the use of a subset of particles to process through the update routine; the use of a library of photon distributions developed from MCNP modeling to estimate the measurement likelihood; and, the implementation of multi-threaded processing techniques to significantly decrease the computation time required for batch processes. Table 4.4, located at the end of this section, outlines the algorithm of the primary processes used to update the posterior distribution by the BASBP.

The posterior update process begins by selecting the subset of particles from the main sample population – this is feature is unique to the BASBP. Unlike the Bayesian particle filtering methods applied a local search operations [10], [37]–[41], the majority of the particles representing the state-space in the BASBP are located in regions a significant distance from any single measurement location. As a result, a cut-off range, R_{cut}, can be selected beyond which the probability of recording a measurement with no portion of the signal attributable to the sources represented by a particle is equal to 1 ($\mathcal{P}(x = 0|\lambda = 0) = 1$). Therefore, there is no need to process these particles through the update routine. Additionally, if a source signal exists, the Poisson distribution will assign a weight of 0 to all particles representing the state in which no source exists ($\mathcal{P}(x = 1|\lambda = 0) = 0$).

Based on R_{cut}, those particles within range of the detector are assigned to the subset $\mathbf{X}^*_{k-1}$, with the corresponding weight and source number vectors, $\mathbf{w}^*_{k-1}$ and $\mathbf{r}^*_{k-1}$, respectively. It is likely that the particle density in the vicinity of a measurement location will be quite sparse. As long as the subset is not empty, the total weight of the subset is recorded and the subset is *resampled* to obtain a new population, $\mathbf{X}^{**}_{k-1}$, of fixed sample size (arbitrarily choosen as

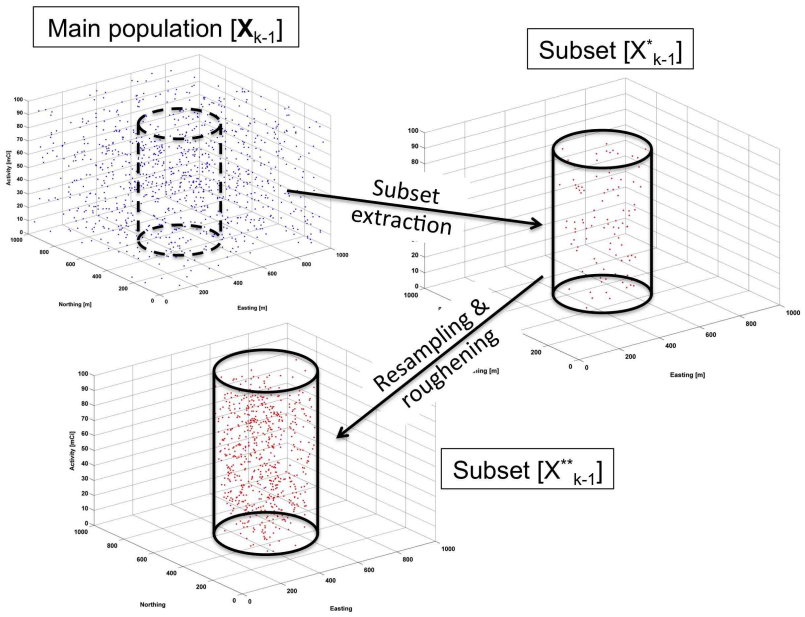

Figure 4.7: Representation of the subset extraction process.

10,000 particles). To avoid degeneracy, the new sample population is *roughend* . Figure 4.7 graphically depicts the process of generating the $\mathbf{X}_{k-1}^{**}$ population.

The process of updating the particle weights in line 7 of Table 4.4 contains the following essential components (note that the BASBP executes this sequence in batches of particles according to the number of sources they represent):

1. Determine the source-detector distance for all of the particles representing s possible sources, $\mathbf{X}_k^{**,s}$.
2. Estimate the total photon flux from the particle's constituent sources based on an empirical fit generated from MCNP models.
3. Calculate the angle between the ground plane and the vector pointing from the source to the detector.
4. Adjust the total photon flux based on Equation 3.13.
5. Estimate the expected counts, $\phi^*(\mathbf{x}^{**,s}, \mathbf{z}_k)$, using the detector parameters.
6. Calculate the measurement likelihood for each particle using: $\mathcal{P}(y_k^{src}|\phi_S^*)$.
7. Update the particle weights based on Equation 3.18: $w_t = w_{t-1} \cdot \mathcal{G}(y_t|x_i(t))$.

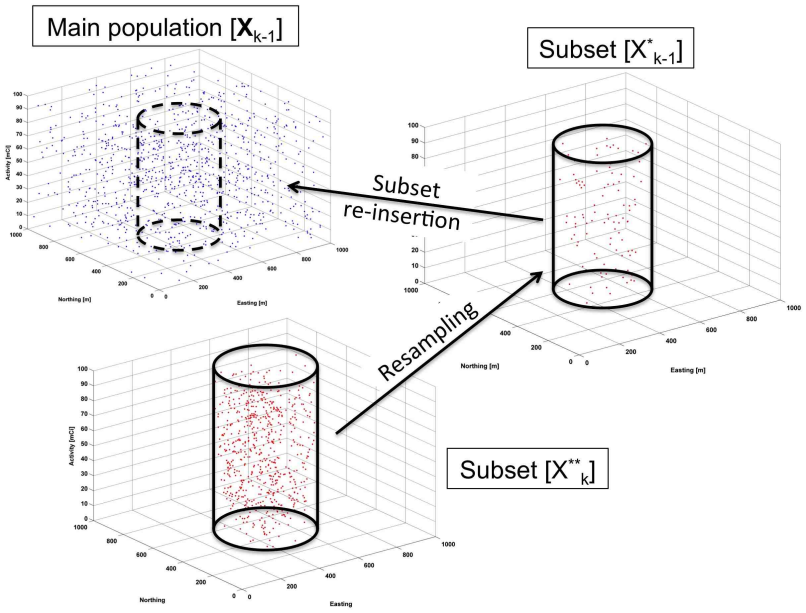

Figure 4.8: Representation of the subset re-insertion process.

8. Normalize the weights, $\mathbf{X}_k^{**,s}$
9. *Resample & roughen* $\mathbf{X}_k^{**,s}$

Once the sequence has looped through the range of possible sources numbers, the entire $\mathbf{X}_k^{**,s}$ population is once again *resampled*. However, only enough samples are drawn to return the population to the size of the original subset, $\mathbf{X}_{k-1}^{*}$. Prior to re-inserting the subset back into the main particle distribution as $\mathbf{X}_k$, the weight factor recorded when the particles were originally extracted from $\mathbf{X}_{k-1}$ is applied. This process ensures that extraction and re-insertion process does not skew the global population. Figure 4.8 depicts the process of returning the particle subset to the main population.

Once the posterior update process is complete, parameter estimates proceed as developed in Section 3.4. Additional products, such as a spatial distribution map, can be generated by tallying particle weights on a gridded mesh.

Table 4.4: Posterior Update Algorithm

Line	Process
1 :	**Subroutine** Posterior Update $([\mathbf{X}_{k-1}^n, \mathbf{r}_{k-1}^n, \mathbf{w}_{k-1}^n]_{n=1}^N, y_k, \widehat{BG}_k, \tau_k)$
2 :	Find subset of particles, $\mathbf{X}_{k-1}^*$, within 200m of y_k.
3 :	**For** all $\mathbf{X}_{k-1}^n \ni \mathbf{X}_{k-1}^*$: **If** $y_k > 0, \mathbf{w}_{k-1}^n = 0$.
4 :	Find weight fraction of subset $\mathbf{X}_{k-1}^*$: $f_{w^*} = \sum_n^{N1} \mathbf{w}_{k-1}^n$.
5 :	Create subset of size N2. $[\mathbf{X}_{k-1}^{**}, \mathbf{r}_k^{**}, \mathbf{w}_{k-1}^{**}] =$ **Resample** $[\mathbf{X}_{k-1}^*, \mathbf{r}_k^*, \mathbf{w}_{k-1}^*]$
6 :	**Do** $s = 0$, s_{max}
7 :	$\mathbf{w}_k^{**,s} = \mathbf{w}_{k-1}^{**,s} \cdot p(y_k \vert \widehat{BG}_k, \mathbf{X}_{k-1}^{**,s})$
8 :	Normalize $\mathbf{w}_k^{**,s}$.
8 :	**Resample**$[\mathbf{X}_k^{**,s}, \mathbf{w}_k^{**,s}]$.
9 :	**Roughen**$[\mathbf{X}_k^{**,s}]$ in space.
10 :	**End Do**
11 :	Create subset of size N1: $\mathbf{X}_k^* =$ **Resample**$[\mathbf{X}_k^{**}, \mathbf{r}_k^{**}, \mathbf{w}_k^{**}]$
12 :	Normalize $\mathbf{w}_k^{**}$ to f_{w^*}.
13 :	Move $\mathbf{X}_k^*$ into $\mathbf{X}_k$, $\mathbf{r}_k^*$ into $\mathbf{r}_k$, and $\mathbf{w}_k^*$ into $\mathbf{w}_k$.
14 :	**End Subroutine** Posterior Update

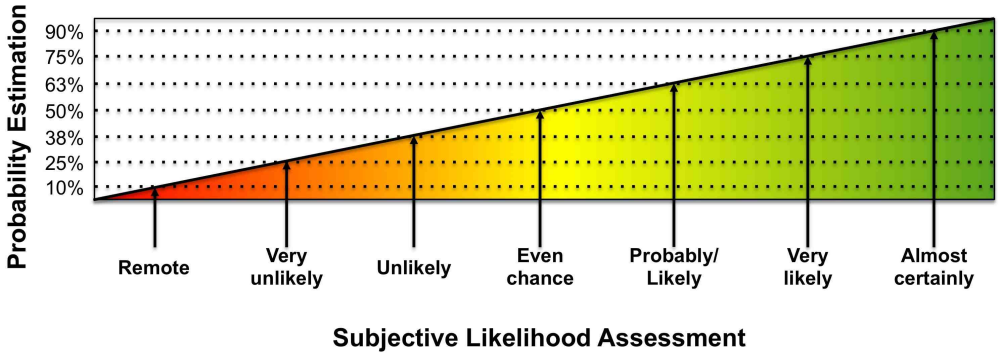

Figure 4.9: Probability estimation from subjective likelihood assessments.

4.5 Geo-spatial Data Fusion

Within the last decade, an entire industry has emerged centered around geo-spatial data mining, analysis and fusion in an effort to cope with exponential increases in the volume of electronic data available in the government, commercial industry, and private sectors. While the focus herein is on the development and utility of the BASBP, the fact is worth highlighting that operating in probability space with respect to interpreting the data streaming from radiation detection platforms offers a clean framework within which one can fuse detector information with data from disparate sources.

The argument here is that any information which suggests the likelihood of any of the unknown parameters of interest (source location, intensity, and source type) can be formed into a probability distribution and used to filter particles. The justification is two-fold. First, it is common practice within the law enforcement and intelligence communities to assign a subjective assessment of the probability (or likelihood) associated with analytical conclusions based on intelligence data. While the intelligence community is loathe to do so, Figure 4.9 depicts the mapping of the the probabilistic language used in assessments to likelihood values [42].

The second argument for conducting data fusion in probability space is based on the simple fact that probability provides a common frame of reference between different data types. Analytical methods applied to the geo-tagged data from disparate sensors and sensor

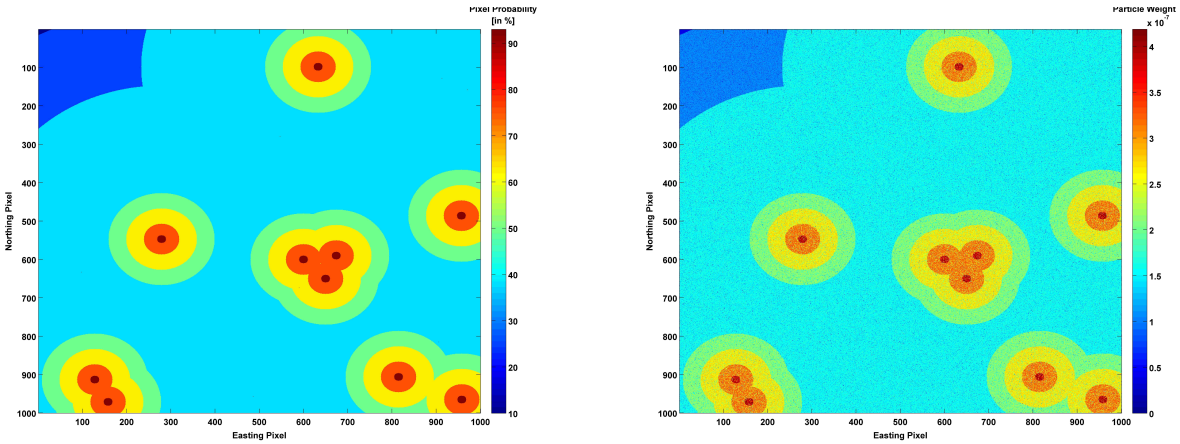

(a) Generic example of an spatial likelihood filter.

(b) Example of passing uniformly drawn particles through a spatial filter.

Figure 4.10: Depiction of the use of geo-spatial data as a particle filter.

types can yield spatial probability distributions. It is not proposed that the BASBP conduct the analysis of any data other than that streaming from radiation detectors. Rather, the observation made here is that a logical point of injecting a filter based on outside data exists after the BASBP has completed the posterior updating process.

Figure 4.10a depicts a generic example of a notional analytical product based on some form of geo-spatial data that represents the spatial likelihood distribution associated with the theft of a radiation source. Applying the same technique used to development the spatial *prior* distribution used by the BASBP, each pixel in a spatial filter image is tagged with its associated likelihood. Figure 4.10b shows the results after passing 10 million particles (drawn uniformly in space) thru the spatial filter (the high number of particles is used only demonstrate the fidelity of the process).

In practice, the only requirements placed on the geo-spatial filter are: the pixel likelihoods must be normalized to 1; and, the filtering image must at least cover the spatial domain occupied by BASBP particles. Implementation of the data fusion process in the BASBP takes the form of an additional *resampling*, normalization, and *roughening* sequence.

4.6 Providing Sensor Guidance

Bayesian optimization of available resources occurs when the updated posterior distribution is coupled with a sensor guidance routine capable of suggesting the location for the next iteration of measurements that has the highest payoff. With robotics and unmanned aerial vehicles fairly common place in modern times, a large body of work documents the research devoted to the topic of sensor management and guidance. Because sensor guidance plays an important role in the employment of remotely operated systems, the outline here focuses on an approach that employs the knowledge gained from Bayesian methods. In the continuation of this research, a proposed way ahead leverages the procedures outlined by Ristic (et al) to provide sensor guidance to the radiation detection platforms executing the broad-area search [10].

Use of the Rényi divergence between the the current posterior distribution and projected posterior distributions provides the means to construct an appropriate reward function. Maximization of the reward function selects the optimum sensor location for the next measurement. Ristic (et al) approximate the expected reward according to Equation 4.11:

$$E\left[\mathcal{R}(\mathbf{u}_k^d, \mathbb{P}(\mathbf{X}_k))\right] \approx \frac{1}{\alpha - 1} \sum_{y=Y_1^*}^{Y_2^*} \gamma_1(y_{k+1}^d|\mathbf{u}_k^d) \ln\left[\frac{\gamma_\alpha(y_{k+1}^d|\mathbf{u}_k^d)}{\gamma_1(y_{k+1}^d|\mathbf{u}_k^d)^\alpha}\right] \tag{4.11}$$

where $\mathbf{u}_k^d$ is the control vector containing the coordinates of a proposed location for detector d, $\mathbb{P}(\mathbf{X}_k)$ represents the current posterior distribution of particles, α is a fixed constant that controls the emphasis placed on the tails of the distributions, y_{k+1}^d the predicted value of a future measurement, y (where $y \in \{Y_1^*, \ldots, Y_2^*\}$, and the function $\gamma_\alpha(y_{k+1}^d|\mathbf{u}_k^d)$ is given by:

$$\gamma_\alpha(y|\mathbf{u}_k^d) = 1/N \sum_{n=1}^{N} \pi(y|\mathbf{X}_k)^\alpha \tag{4.12}$$

where $\pi(y|\mathbf{X}_k)$ is posterior distribution evaluated at y. In theory, the set of proposed measurement locations is continuous and the range of projected measurement values is infinite. To simplify the process and increase the speed of execution, a finite set can be

defined, $\mathbf{u}_k^d$, to contain the four cardinal positions located 50m from the current measurement. Further, the set of predicted values can be restricted by setting $Y_1^* = y_{\min}$ and $Y_2^* = y_{\max}$ and to include two additional sample points at 1/3 and 2/3 of the range. The functionality of such an approach remains to be seen.

5 | Simulated BASBP Performance

The bulk of this research, centered exclusively around the development of the BASBP, focuses on implementing the Bayesian methods in the FORTRAN programming language and data manipulation. In the absence of an aerial detection system collecting against a known source, the demonstration of aspects of the BASBP's performance relies on the collection and processing of real-world geo-spatial, the production of *priors*, the processing of radiation survey data as reported by others, and an examination of how the BASBP handles the information.

5.1 Performance of the BASBP Detection Decision Function

Because the detection decision serves as the foundation of all of the subsequent core BASBP processes, a simulated test of the algorithm was performed using the expected signal from a notional, 4 mCi Cs-137 point source and aerial survey data collected by the Aerial Measuring Systems-Remote Sensing Laboratory RSX-3 system collected over the Presidio, CA [26], [43]. The following elements characterize the radiological survey mission:

- Location: Presidio, CA
- Sources: None
- Platform: RSL Bell-412 helicopter
- Detector: 12 NaI(Tl) detectors assembled into 4 pods.
- Flight plan: standard grid pattern flown at altitudes between 50 m and 150 m and a ground speed of roughly 70 knots.

Figure 5.1 depicts the total counts (background and when combined with the injected signal), the injected counts, and the detection decision as a function of measurement number. While the bottom plot in Figure 5.1a clearly shows the spike in the detection decision, Figure 5.1b depicts a close-up view of the data in the vicinity of the declared detection event.

Figure 5.2 depicts the flight path used in the aerial survey. The measurement locations for which no source is declared are depicted in blue and the locations where a detection event is declared are depicted in green. The notional 4 mCi Cs-137 source is depicted by the red asterisk, located approximately at the center mass of the search area. This graphic further depicts the variability of the terrain according to land-use category – clearly evident are the false-positives declared when significant changes in the terrain occur.

To compare the detection decision function used by the BASBP to a more conventional approach of estimating of the background, consider the case where a 20-point rolling estimate is used and the threshold for detection is set at 3-σ. The top graph in Figure 5.3 depicts the estimated signal (measured signal with the injected 4 mCi Cs-137 signal) in blue and the 20-point rolling average in red as functions of measurement number. To correlate the measurements to spatial locations, measurement number 1 occurs where the flight path enters Figure 5.2 from the right. Evident in Figure 5.3 are the turns executed over water (where the minimums counts occur) as well as the turns executed over land (prominent v-notches). The bottom graph depicts the frequency of detection calls based on the 3-σ threshold. Clearly, although the method correctly triggers a detection event at measurement 1216 as the BASBP, numerous false alarms are declared due to spatial deviations in the background.

Exploring the possibility of using a more restrictive rolling-average estimate of the background, Figure 5.4 depicts the case in which a 5-point estimate is used for varying detection decision thresholds (3-, 10-, 17-, and 24-σ, from top to bottom). While setting a higher threshold on the detection decision reduces the number of false positives, extreme thresholds also have the effect of increasing the likelihood of a false negatives. It is clear that setting a higher detection decision threshold is not an effective means to compensate for the lack of knowledge regarding the variability of the background.

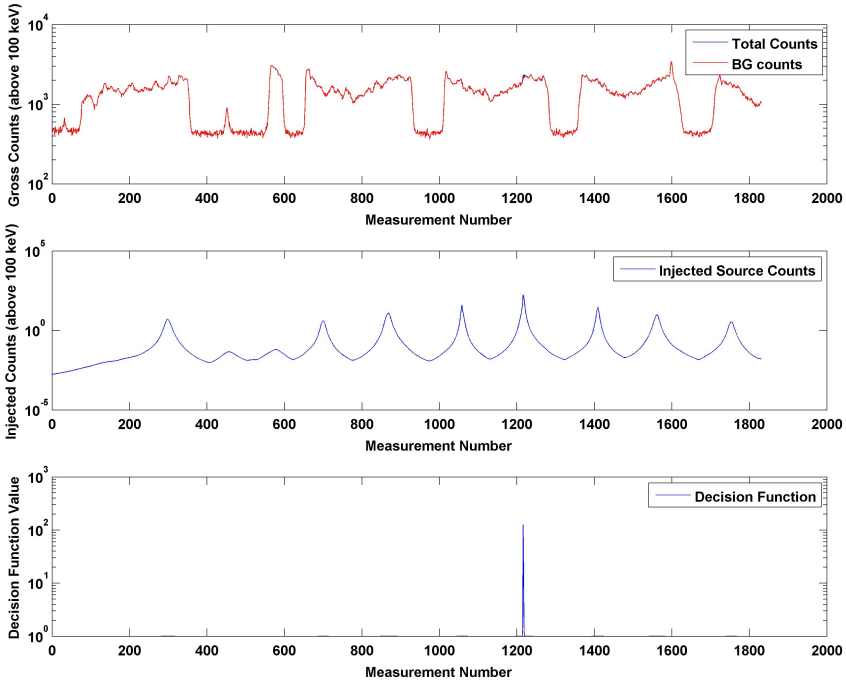

(a) Full range of the data.

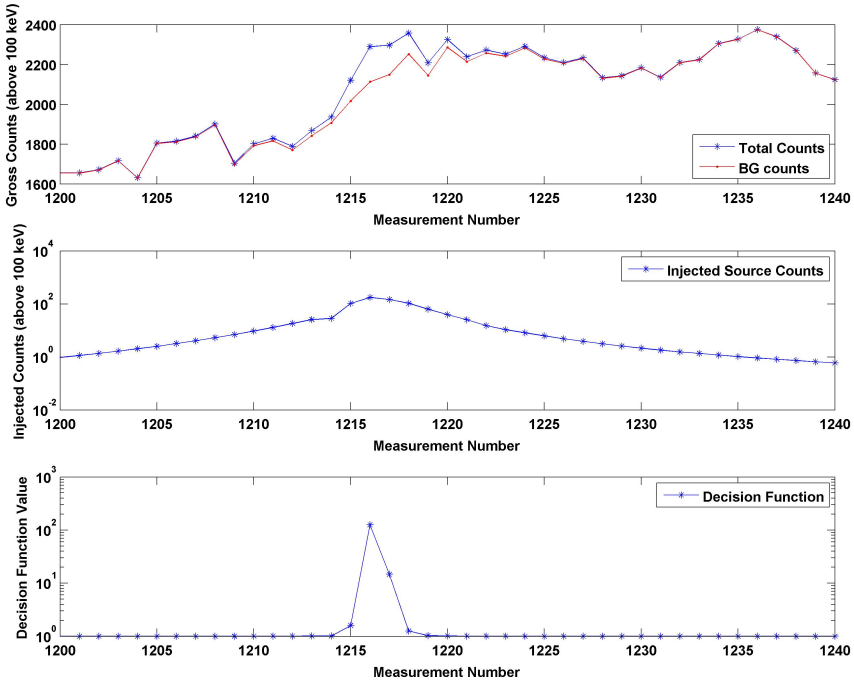

(b) Close-up view of data in the region of the detection decision.

Figure 5.1: Testing of the BASBP Decision Function.

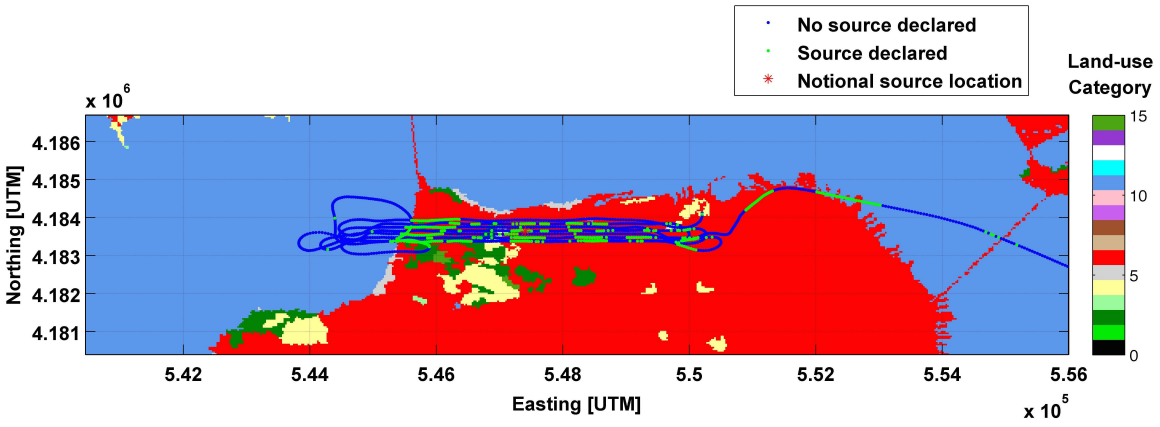

Figure 5.2: Flight path and notional detection decision using injected source (4 mCi Cs-137).

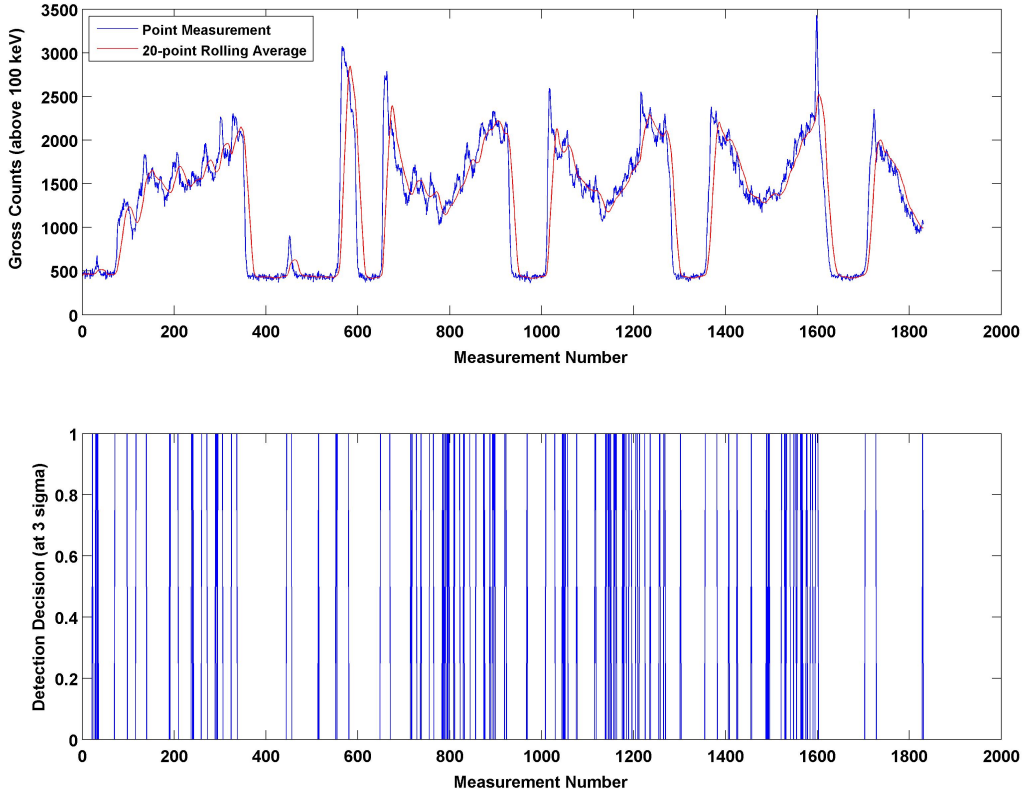

Figure 5.3: Conventional analysis of the Presidio data and corresponding detection decisions using 20-point rolling average and 3-σ threshold.

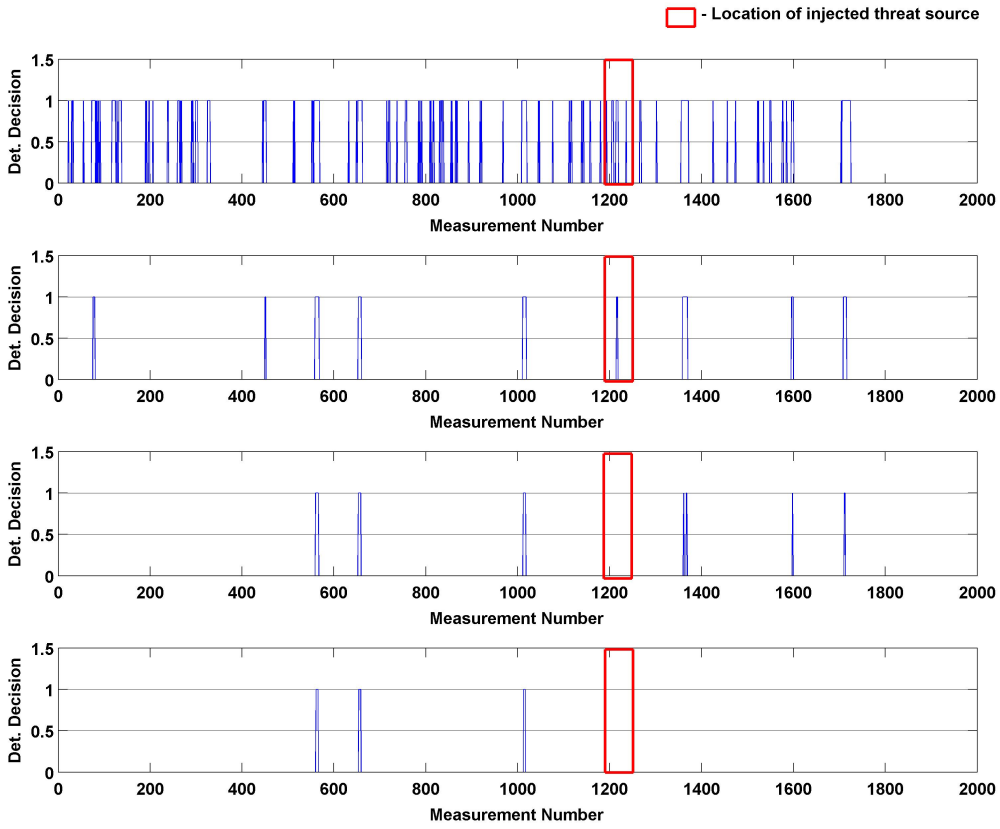

Figure 5.4: Detection decisions using 3-, 10-, 17-, and 24-σ and a rolling 5-point average for the background estimate.

5.2 Initial Evaluation of the BASBP

The evaluation of the initial BASBP performance uses the data collected by the Multi-sensor Aerial Radiation Survey (MARS) system in June of 2012 [44]. Figures presented in Appendix C depicted the elevation data, land-use data, and satellite imagery of the test site. From the technical report published by the Pacific Northwest National Laboratory, the following elements characterize the challenge presented to the MARS system (mounted on a helicopter):

- Location: Desert Rock Airport, NV (near the Nevada National Security Site)
- Sources: Cs-137 (25.3 mCi), Co-60 (4.13 mCi), Ba-133 (7.05 mCi), and Am-241 (18.86 mCi)
- Platform: RSL Bell-412 helicopter
- Detector: 14 HPGe crystals mounted in a single cryostat (for more details on the MARS system see [45])
- Flight plan: multiple passes at altitudes of 50, 100, 150, 200, 300, and 500 feet at 70 knots ground speed.

Figure 5.5 depicts the comparison between the total counts collected above 100 keV during passes at approximately 10 m and 100 m. Note that the measurement numbers are not assigned according to platform position, but the alignment is readily apparent. For clarity, the total counts are depicted with a line whereas the data clearly stems from a discrete set of measurement points. The complex nature of the detection system precluded the use of the complete data set as it is possible that photons scattered by the detection system are recorded in multiple crystals as single events. In order to run this data set thru the BASBP, one would need to know the detector response function in greater detail in order to map the total counts recorded to the number of incident photons. In lieu of using the data points clearly attributable to the radiation sources, Figure 5.6 demonstrates the BASBP by showing the initial particle population, the results after stripping the source data from the set, and finally, a trial run attempting to use the data as is.

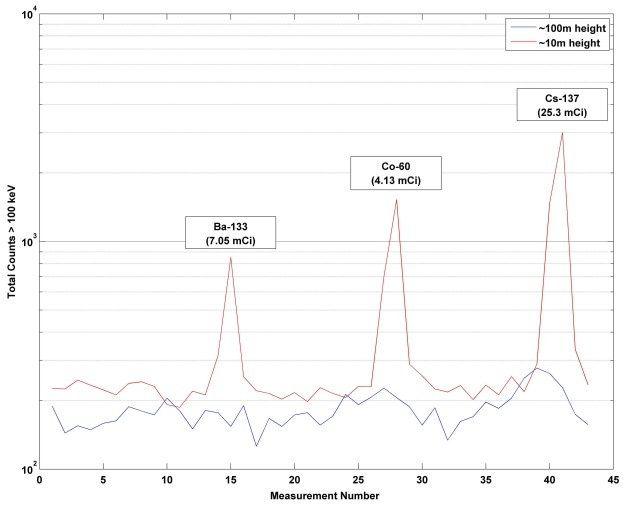

Figure 5.5: Representative data collected by the MARS system, June 2012.

As depicted in (Figure 5.6a), the initial particle populations clearly represents the probability distribution generated from the land-use categories depicted in Figure C.3. Running the BASBP without the data points attributable to the point sources included, the BASBP strips particles from area overflown by the detection platform (void in the center of the scene, Figure 5.6b). In the case of attempting to run the full data set through the BASBP with the source data points intact, an undermined error in data processing currently terminates execution just after the system detects the maximum Ba-133 peak. However, note that a particle cluster appears just off the airfield when this occurs (Figure 5.6c). It is possible that the problem in the code is attempting to maintain particles capable of generating the estimated source signal.

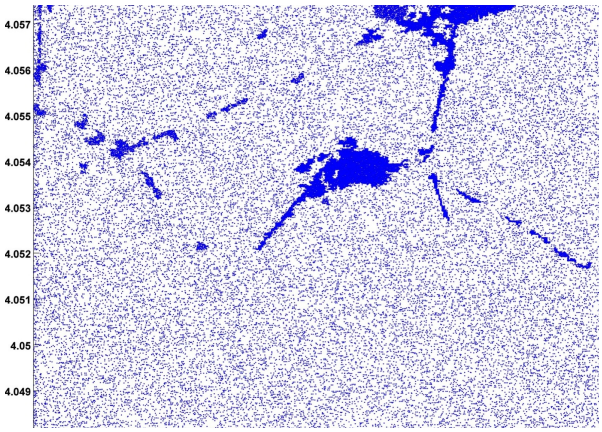

(a) Intial particle population.

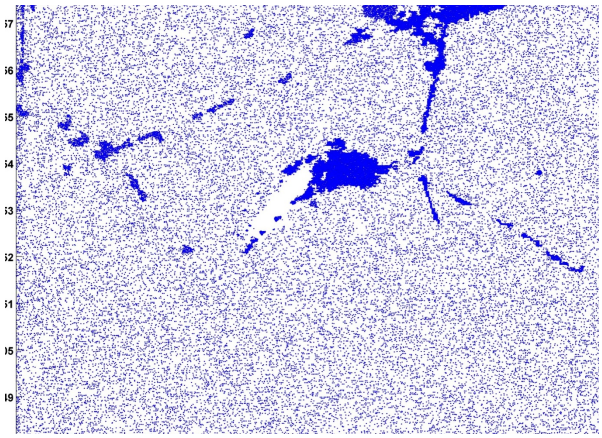

(b) Trial with no source data points.

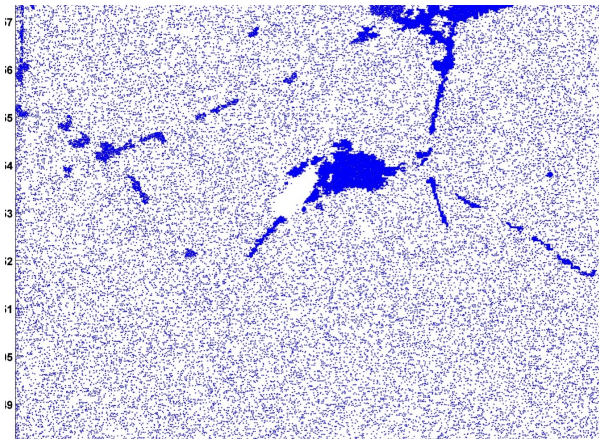

(c) Trial with source data points.

Figure 5.6: Examples of the spatial distribution of BASBP particle populations.

6 | Conclusions and Future Work

Faced with the proverbial challenge of finding a needle in a haystack, the application of Bayesian signal processing methods to the broad-area search problem shows great promise. While much work remains, the following key attributes are demonstrated in the BASBP: the ability to leverage radiation transport physics; the ability to ingest geo-spatial data to create both functional *priors* and conduct data fusion; the ability to rapidly process a large particle population size; and, the ability to discriminate between a potential threat source and a location varying background signal with a significantly lower false-positive rate.

Lacking an aerial detection platform, no claim is made as to the range at which detection distances are expected to increase by employing the BASBP. The inclusion of radiation transport physics in the broad-area search model, while the BASBP processes detector data in real time, is a significant accomplishment. While neither Bayesian methods nor the process of building libraries using MCNP are new concepts, this is the first demonstration of the process of combining both methods in the context of a broad-area search algorithm.

In terms of Bayesian particle filtering methods, two components are absolutely critical: construction of the *priors* and sampling methods employed. This research demonstrated the ability of the BASBP core program to transform geo-spatial data into accurate and meaningful *priors*. Despite the volume of data ingested, efficient BASBP processes rapidly transform geo-spatial datasets into probability distributions. When geo-spatial data is applied to the back end of the BASBP process (following the *posterior update*), prospects exist for data fusion to serve as an additional particle filtering method. Additionally, the ability to operate in probability-space affords tremendous opportunities to combine disparate types of information and provides the framework for true, all-source data fusion.

While not highlighted elsewhere, optimization of the BASBP core processes by leveraging multi-core processes significantly increases the applicability of the program to the broad-area search problem. Employing particle filtering techniques across a spatial domain that greatly

exceeds the extend of the signals measured requires large particle populations. Benchmarking a non-optimized BASBP posterior update routine against the same routine written to exploit parallel processing shows a reduction in processing time of nearly 2 orders of magnitude.

Although this research was constrained to aerial data sets made available by others, the detection decision serves as the central function every detection system must perform. The BASBP's ability to provide a detection decision when given a location varying background serves as one of its primary features.

The continued development of this research should follow three main tracks. First, the continued development and refinement of the core BASBP processes will significantly improve the code. Much work remains to be done on the back end of the processes to ease the burden of post-processing and bring the BASBP closer to an operational system. While a proposed way forward exists regarding the sensor guidance routine, more research is required to select the most appropriate method for determining future measurement locations based on Bayesian risk-reward analysis.

The second primary track along which this research should advance is the development of a low-cost, unmanned, aerial detection platform. While the initial process of designing an aerial system to couple with the BASBP system via RF communications has started, much work remains. As currently envisioned, the BASBP will operate from a ground control station to provide situational awareness and sensor guidance recommendations to platform controller. However, the primary challenge during the design phase will be finding the optimal balance of between flight time, system performance, the means to link the BASBP to a live data stream.

Broad-area modeling is the third thrust area this research should initiate. The 1D modeling performed to build an initial library for the BASBP supports the conclusion that the broad-area search requires a model that includes radiation transport physics. However, it remains to be seen whether or not efficient estimated flux libraries libraries can be generated from higher fidelity radiation transport models of the problem space.

Bibliography

[1] D. Rumsfeld, *Quadrennial Defense Review Report*, Washington D.C.: Department of Defense, 2006.

[2] R. M. Gates, *Quadrennial Defense Review Report*, Washington D.C.: Department of Defense, 2010.

[3] D. M. D'Agostino, "Weapons of Mass Destruction: Actions Needed to Track Budget Execution for Counterproliferation Programs and Better Align Resources with Combating WMD Strategy," United States Government Accountability Office, Report GAO-10-755R, 2010.

[4] United States, Department of the Army, *Concept Capability Plan for Combating Weapons of Mass Destruction for the Future Modular Force 2015-2024*, ser. TRADOC Pamphlet 525-7-19. Fort Eustis: Training and Doctrine Command, 2009.

[5] H. Gowadia, "Keeping America Secure: The Science Supporting the Development of Threat Detection Technologies," Statement to the House, Committee on Science, Space, and Technology (Serial 112-97), 19 July 2012.

[6] G. Vavrina and J. Greaves, "Nuclear Disablement Team in Operation Iraqi Freedom: Part II," *NBC Report*, pp. 25–30, 2004.

[7] J. Candy, D. Chambers, E. Breitfeller, B. Guidry, J. Verbeke, M. Axelrod, K. Sale, and A. Meyer, "Threat detection of radioactive contraband incorporating compton scattering physics: A model-based processing approach," *IEEE Transactions on Nuclear Science*, vol. 58, pp. 214–230, Feb. 2011.

[8] X. Qingpei, T. Dongfeng, Z. Jianyu, H. Fanhua, D. Ge, and Z. Jun, "Numerical study on the sequential bayesian approach for radioactive materials detection," *Nuclear Instruments and Methods in Physics Research Section A: Accelerators, Spectrometers, Detectors and Associated Equipment*, vol. 697, pp. 107–113, 2013.

[9] K. D. Jarman, E. A. Miller, R. S. Wittman, and C. J. Gesh, "Bayesian radiation source localization," *Nuclear Technology*, vol. 175, no. 1, pp. 326–334, July 2011.

[10] B. Ristic, M. Morelande, and A. Gunatilaka, "Information driven search for point sources of gamma radiation," *Signal Processing*, vol. 90, no. 4, pp. 1225 – 1239, 2010.

[11] United States, Census Bureau, "TIGER Products," Online Database, 2013. [Online]. Available: www.census.gov/geo/maps-data/data/tiger.html

[12] International Atomic Energy Agency, "Illicit Trafficking and Other Unauthorized Activites Involving Nuclear and Radioactive Materials," Fact Sheet, 2005. [Online]. Available: www-ns.iaea.org/downloads/security/itdb-fact-sheet.pdf

[13] National Nuclear Data Center, "Chart of the Nuclides," Brookhaven National Laboratory, Online application, 2014. [Online]. Available: http://www.nndc.bnl.gov/chart/

[14] D. B. Pelowitz, "MCNP6 User's Manual," Las Alamos National Laboratory, Manual LA-CP-11-01708, 2012.

[15] C. G. Wahl, "Imaging, Detection, and Identification Algorithms for Position-Sensitive Gamma-Ray Detectors," Ph.D. dissertation, University of Michigan, 2011.

[16] K. P. Ziock and W. H. Goldstein, "The lost source, varying backgrounds and why bigger may not be better," in *Unattended Radiation Sensor Systems for Remote Applications*, J. I. Trombka, Ed., vol. 632, no. 1, 2002, pp. 60–75.

[17] K. P. Ziock, W. W. Craig, L. Fabris, R. C. Lanza, S. Gallagher, B. Horn, and N. Madden, "Large Area Imaging Detector for Long-Range, Passive Detection of Fissile Material," *IEEE Transactions on Nuclear Science*, vol. 51, no. 5, pp. 2238–2244, 2004.

[18] K. P. Ziock, J. W. Collins, L. Fabris, S. Gallagher, B. Horn, R. C. Lanza, and N. W. Madden, "Source-search sensitivity of a large-area, coded-aperture, gamma-ray imager," *IEEE Transactions on Nuclear Science*, vol. 53, no. 3, pp. 1614–1621, 2006.

[19] K. P. Ziock, L. Fabris, D. Carr, J. Collins, M. Cunningham, F. Habte, T. Karnowski, and W. Marchant, "A Fieldable-Prototype, Large-Area, Gamma-Ray Imager for Orphan

Source Search," *IEEE Transactions on Nuclear Science*, vol. 55, no. 6, pp. 3643–3653, Dec 2008.

[20] K. Vetter, L. Mihailescu, K. Nelson, J. Valentine, and D. Wright, "Gamma-ray Imaging Methods," Lawrence Livermore National Laboratory, Technical Report UCRL-TR-225239, 2006.

[21] L. Schultz *et al.*, "Hybrid Coded Aperture and Compton Imaging using an Active Mask," *Nuclear Instruments and Methods in Physics Research Section A*, vol. 608, no. 2, pp. 267 – 274, 2009.

[22] S. Zelakiewicz, R. Hoctor, A. Ivan, W. Ross, E. Nieters, W. Smith, D. McDevitt, M. Wittbrodt, and B. Milbrath, "SORIS—A standoff radiation imaging system," *Nuclear Instruments and Methods in Physics Research Section A: Accelerators, Spectrometers, Detectors and Associated Equipment*, vol. 652, no. 1, pp. 5 – 9, 2011.

[23] E. E. Lewis and W. F. Miller Jr., *Computational Methods of Neutron Transport*. La Grange Park, IL: American Nuclear Society, Inc., 1993.

[24] R. E. Pevey, "NENG 583: Radiation Transport Methods," University of Tennessee, Course Notes, 2011.

[25] Glenn F. Knoll, *Radiation Detection and Measurement*, 3rd ed. New York: John Wiley & Sons, Inc., 2000.

[26] National Security Technologies, "An Aerial Radiological Survey of the King and Pierce Counties, Washington," Aerial Measuring Systems, Remote Sensing Laboratory, Technical Report N18765, 2011. [Online]. Available: www.doh.wa.gov/Portals/1/Documents/4100/aerialsurvtech_p_.pdf

[27] T. Ulvsand, B. Lauritzen, and R. R. Finck, "NKS/SRV Seminar on Barents Rescue 2001 LIVEX. Gamma Search Cell," Nordic Nuclear Safety Research, NKS Secretariat, P.O. Box 49, DK-4000 Roskilde, Denmark, Report NKS-54, 2002.

[28] J. Candy, *Bayesian Signal Processing: Classical, Modern, and Particle Filtering Methods*. Hoboken: John Wiley & Sons, 2009.

[29] J. K. Ghosh, M. Delampady, and T. Samanta, *An Introduction to Bayesian Analysis*, ser. Springer Texts in Statistics. New York: Springer, 2006.

[30] C. P. Robert, *The Bayesian Choice*, 2nd ed., ser. Springer Texts in Statistics. New York: Springer, 2007.

[31] N. Gordon, D. Salmond, and A. F. M. Smith, "Novel Approach to Nonlinear/Non-Gaussian Bayesian State Estimation," *IEE Proceedings F: Radar and Signal Processing*, vol. 140, no. 2, pp. 107–113, 1993.

[32] P. Stavropoulos and D. M. Titterington, *Sequential Monte Carlo Methods in Practice*. New York: Springer, 2001, ch. Impoved Particle Filters and Smoothing.

[33] C. Musso, N. Oudjane, and F. LeGland, *Sequential Monte Carlo Methods in Practice*. New York: Springer, 2001, ch. Improving Regularized Particle Filters.

[34] United States, National Geospatial-Intellegence Agency, "MSP GEOTRANS 3.3," source code, 2013. [Online]. Available: earth-info.nga.mil/GandG/geotrans/index.html

[35] A. L. Mitchell, J. D. Borgardt, and R. T. Kouzes, "Skyshine Contribution to Gamma Ray Background Between 0 and 4 MeV," Pacific Northwest National Laboratory, Tech. Rep. PNNL-18666, Aug 2009.

[36] United States, Department of the Army, Corps of Engineers, "Common Map Background," Army Geospatial Center, Digital Library, 2014. [Online]. Available: www.agc.army.mil/home.aspx

[37] M. Morelande and B. Ristic, "Radiological source detection and localisation using bayesian techniques," *IEEE Transactions on Signal Processing*, vol. 57, pp. 4220–4231, Nov. 2009.

[38] B. Ristic, M. Morelande, and A. Gunatilaka, "A controlled search for radioactive point sources," in *11th International Conference on Information Fusion*, 2008, Conference, pp. 1–5.

[39] B. Ristic, M. Morelande, A. Gunatilaka, and M. Rutten, "Search for a radioactive source: Coordinated multiple observers," in *3rd International Conference on Intelligent Sensors, Sensor Networks and Information*, 2007, pp. 239–244.

[40] B. Ristic, A. Gunatilaka, and M. Rutten, "An information gain driven search for a radioactive point source," in *10th International Conference on Information Fusion*, 2007, pp. 1–8.

[41] M. Morelande, B. Ristic, and A. Gunatilaka, "Detection and parameter estimation of multiple radioactive sources," in *10th International Conference on Information Fusion*, 2007, Conference, pp. 1–7.

[42] United States, Office of the Director of National Intelligence, "Global Water Security," Intelligence Community Assessment ICA 2012-08, 2012. [Online]. Available: www.dni.gov/files/documents/Newsroom/PressReleases/ICA_GlobalWaterSecurity.pdf

[43] K. Vetter, D. Chivers, M. Bandstra, V. Negut, J. Kua, and M. Quinlan, "Gamma-Ray Data Cloud," Lawrence Berkeley National Laboratory, Database, 2013. [Online]. Available: grdc.nersc.gov

[44] S. C. Stave, K. E. Dorow, B. D. Glasgow, J. M. Benz, and J. A. Willett, "MARS June 2012 Flight Data: Natural Background and Point Source Spectra," Pacific Northwest National Laboratory, Technical Report PNNL-21978, Nov 2012. [Online]. Available: http://www.osti.gov/scitech/servlets/purl/1113622

[45] J. E. Fast *et al.*, "The Multi-sensor Airborne Radiation Survey (MARS) Instrument," *Nuclear Instruments and Methods in Physics Research Section A*, vol. 698, no. 0, pp. 152 – 167, 2013.

[46] International Atomic Energy Agency, "Categorization of radioactive sources," International Atomic Energy Agency, IAEA Safety Standards Series RS-G-1.9, 2005.

[47] R. E. Pevey, "NENG 582: Monte Carlo Analysis," University of Tennessee, Course Notes, 2012.

[48] S. A. Dupree and S. K. Fraley, *A Monte Carlo Primer*. New York: Kluwer Academic/Plenum Publishers, 2002.

[49] A. Doucet, N. deFreitas, and N. Gordon, *Sequential Monte Carlo Methods in Practice*, ser. Statistics for Engineering and Information Science, A. Doucet, N. deFreitas, and N. Gordon, Eds. New York: Springer, 2001.

Appendices

Appendix A | Radiation Source Data

This appendix contains basic information regarding radiation sources. Section A.1 provides a list of commonly used sources of radiation, typical applications, activity ranges, and the IAEA threat category. In Section A.2, we provide tables containing basic data supporting the photon signatures associated with nuclear MOC (both conventional sources and SNM). In the case of the SNM sources listed, we estimate the activity levels by aging the composite material by five years and running Monte Carlo estimations of the fraction of the photons born within 1SQ of material that escape without colliding. The graphical depictions of the complete expected spectra from SNM are provided in Section A.3.

A.1 Common Sources of Radiation

Table A.1: Common Uses of Conventional Sources of Radiation

Isotope	Use	Activity [Ci]		Max IAEA Category*
		Min	Max	
Am-241	Industrial gauges	1.20E-02	6.00E-01	4
	Nuclear medicine	2.70E-02	2.70E-01	4
	Industrial static reduction	3.00E-02	1.10E-01	4
	Lightning arrestors	1.30E-03	1.30E-02	5
	Smoke detectors	1.00E-06	1.00E-06	5
Cd-109	Nuclear medicine	2.00E-02	2.00E-02	4
	Analytic chemistry	3.00E-02	1.50E-01	5
Cf-252	Industrial gauges	3.00E-05	3.70E-02	3
	Nuclear medicine	8.30E-02	8.30E-02	4
Cm-244	Industrial gauges	2.00E-01	1.00E+00	4
Co-57	Analytic chemistry	5.00E-03	4.00E-02	5

Continued on next page ...

*The IAEA defines radioactive source categories 1–3 as extremely dangerous, very dangerous, and dangerous to humans, respectively. Category 4 and 5 radiological sources as those that are unlikely and very unlikely to be dangerous to humans, respectively. [46]

Table A.1 - Continued

Isotope	Use	Activity [Ci]		Max IAEA Category
		Min	Max	
Co-60	Industrial sterilization	5.00E+03	1.50E+07	1
	Medical sterilization	1.50E+03	3.00E+03	1
	Nuclear medicine	5.00E+00	1.50E+04	1
	Industrial radiography	1.10E+01	2.00E+02	2
	Industrial gauges	5.00E-03	2.60E+00	3
Cs-137	Industrial sterilization	5.00E+03	5.00E+06	1
	Medical sterilization	1.00E+03	1.20E+04	1
	Nuclear medicine	1.00E-02	1.50E+03	1
	Industrial gauges	1.00E-03	4.00E+01	3
Eu-152	Lightning arrestors	1.00E-03	3.00E-02	5
Fe-55	Analytic chemistry	3.00E-03	1.40E-01	5
Gd-153	Nuclear medicine	2.00E-02	1.50E+00	4
H-3	Analytic chemistry	5.00E-02	3.00E-01	5
	Lightning arrestors	2.00E-01	2.00E-01	5
I-125	Nuclear medicine	4.00E-02	4.00E-02	4
I-131	Nuclear medicine	1.00E-01	2.00E-01	4
Ir-192	Industrial radiography	5.00E+00	2.00E+02	2
	Nuclear medicine	2.00E-02	1.20E+01	2
Kr-85	Industrial gauges	5.00E-02	1.00E+00	4
Ni-63	Analytic chemistry	5.00E-03	2.00E-02	5
P-32	Nuclear medicine	6.00E-02	6.00E-01	5
Pm-147	Industrial gauges	2.00E-03	5.00E-02	4
Po-210	Industrial static reduction	3.00E-02	1.10E-01	4
Pu-238	RTGs	2.80E+01	2.80E+02	1
Ra-226	Industrial gauges	2.00E-03	4.00E-03	4
	Nuclear medicine	5.00E-03	5.00E-02	4
	Lightning arrestors	7.00E-06	8.00E-05	5
Se-75	Industrial radiography	8.00E+01	8.00E+01	2
Sr-90	RTGs	9.00E+03	6.80E+05	1
	Industrial gauges	1.00E-02	2.00E-01	4
	Nuclear medicine	2.00E-02	4.00E-02	5
Tm-170	Industrial radiography	2.00E+01	2.00E+02	2
Yb-169	Industrial radiography	2.50E+00	1.00E+01	2

A.2 Photon Signatures Associated with Materials of Concern

Table A.2: Primary Photon Signatures (above 0.1 MeV) from Conventional Sources

Source	Decay Mode	Activity [Ci/gm]	Energy [MeV]	Intensity [#/gm-s]	Mean Free Path [m] in Air	in Al	in Pb
Co-60	β- (100%)	1.1316E+03	1.3325	4.186E+13	159.1	0.070	0.0156
			1.1732	4.181E+13	149.2	0.065	0.0142
			0.8261	3.182E+09	125.7	0.055	0.0103
			0.3471	3.140E+09	86.8	0.038	0.0029
			2.1586	5.024E+08	205.1	0.089	0.0195
Se-75	ϵ (100%)	1.4549E+04	0.2647	3.171E+14	78.4	0.034	0.0017
			0.1360	3.138E+14	62.6	0.026	0.0003
			0.2795	1.345E+14	78.0	0.035	0.0019
			0.1211	9.259E+13	60.4	0.024	0.0003
			0.4007	6.174E+13	91.8	0.040	0.0038
Cs-137	β- (100%)	8.6811E+01	0.6617	2.733E+12	113.6	0.050	0.0079
			0.2835	1.863E+07	80.4	0.035	0.0019
Ir-192	β- (95.24%) ϵ (4.76%)	9.2132E+03	0.3165	2.690E+14	83.7	0.036	0.0024
			0.4681	1.553E+14	97.8	0.043	0.0049
			0.3085	9.643E+13	82.9	0.036	0.0023
			0.2960	9.321E+13	81.6	0.035	0.0021
			0.6044	2.668E+13	109.1	0.048	0.0071
Ra-226	α (100%)	9.8857E-01	0.1862	1.331E+09	69.3	0.029	0.0007
			0.2623	1.829E+06	78.2	0.038	0.0016
			0.6007	1.792E+05	108.7	0.048	0.0071
			0.4146	1.097E+05	93.1	0.041	0.0040
			0.4494	6.950E+04	96.2	0.042	0.0046
Pu-238	α (100%)	1.7124E+01	0.1527	5.886E+06	65.0	0.027	0.0005
			0.1113	1.394E+05	58.8	0.023	0.0002
			0.7664	1.394E+05	121.4	0.053	0.0094
			0.1104	7.350E+04	58.6	0.023	0.0002
			0.1144	5.398E+04	59.3	0.023	0.0002

Table A.3: Primary SNM Photon Signatures (above 0.1 MeV) from 1x Significant Quantity of Material

SNM Type [Ci/gm]	Isotope	Decay Mode(s)	Energy [MeV]	Intensity [#/s]	Mean Free Path [m]			
					Air	Al	Pb	SNM
HEU (0.0989)	U-235	α (100%)	0.1857	8.9006E+07	69.3	0.029	0.0007	0.0003
	U-235	α (100%)	0.1438	1.2765E+07	63.7	0.026	0.0004	0.0002
	U-235	α (100%)	0.2053	8.7025E+06	71.6	0.032	0.0009	0.0004
	U-235	α (100%)	0.1633	6.8452E+06	66.4	0.028	0.0005	0.0002
	U-235	α (100%)	0.1092	2.3496E+06	58.4	0.023	0.0002	0.0003
HEU (w/ ^{232}U) (0.1358)	U-235	α (100%)	0.1857	8.9006E+07	69.3	0.029	0.0007	0.0003
	Tl-208	β- (100%)	2.6145	6.2716E+07	227.2	0.098	0.0202	0.0114
	Tl-208	β- (100%)	0.5832	3.0883E+07	107.4	0.047	0.0068	0.0034
	U-235	α (100%)	0.1438	1.2765E+07	63.7	0.026	0.0004	0.0002
	U-235	α (100%)	0.2053	8.7025E+06	71.6	0.031	0.0009	0.0004
DU (0.0170)	Pa-234m	β- (99.848%)	1.0010	8.5771E+05	62.5	0.026	0.0003	0.0002
	Pa-234m	β- (99.848%)	0.7664	2.8180E+05	56.3	0.021	0.0001	0.0003
	U-235	α (100%)	0.1857	1.9779E+05	69.3	0.029	0.0007	0.0003
	Pa-234m	β- (99.848%)	0.7428	9.2986E+04	56.3	0.021	0.0001	0.0002
	Th-234	β- (100%)	0.1128	5.7121E+04	51.1	0.017	0.0003	0.0001
WGPu (1625.8)	Pu-239	α (100%)	0.1293	6.3039E+07	61.6	0.025	0.0003	0.0001
	Pu-239	α (100%)	0.4137	4.8612E+07	91.0	0.041	0.0040	0.0018
	Pu-239	α (100%)	0.3751	4.7542E+07	89.4	0.039	0.0034	0.0015
	Pu-240	α (100%)	0.1042	2.3809E+07	57.6	0.022	0.0002	0.0003
	Pu-239	α (100%)	0.1113	2.0913E+07	58.8	0.023	0.0002	0.0003

A.3 SNM Photon Signatures

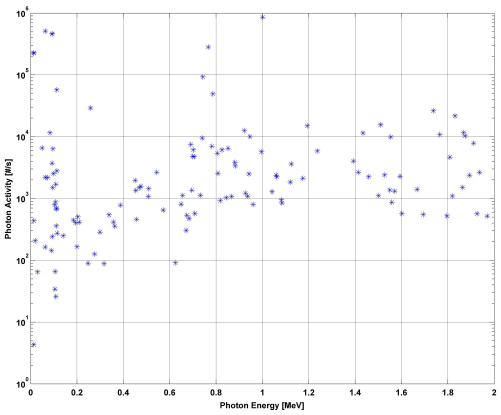

(a) Depleted uranium.

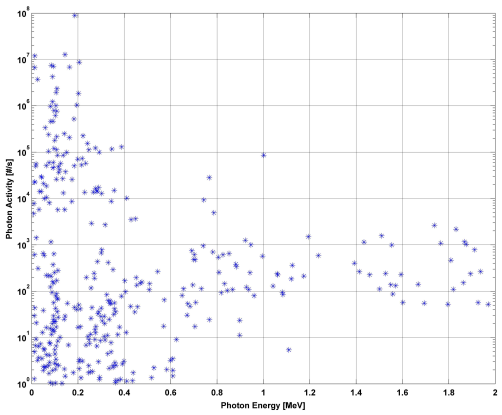

(b) HEU.

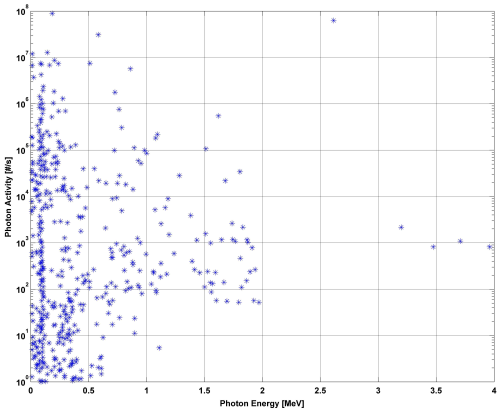

(c) HEU with trace U-232.

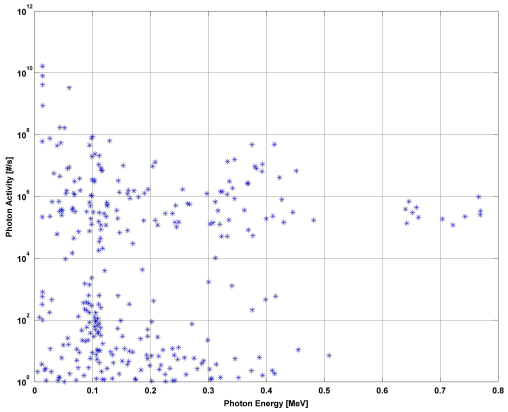

(d) Weapons-grade Plutonium.

Figure A.1: Estimated Photon Spectra from 1SQ SNM, aged 5 years.

A.4 Photon Flux Data

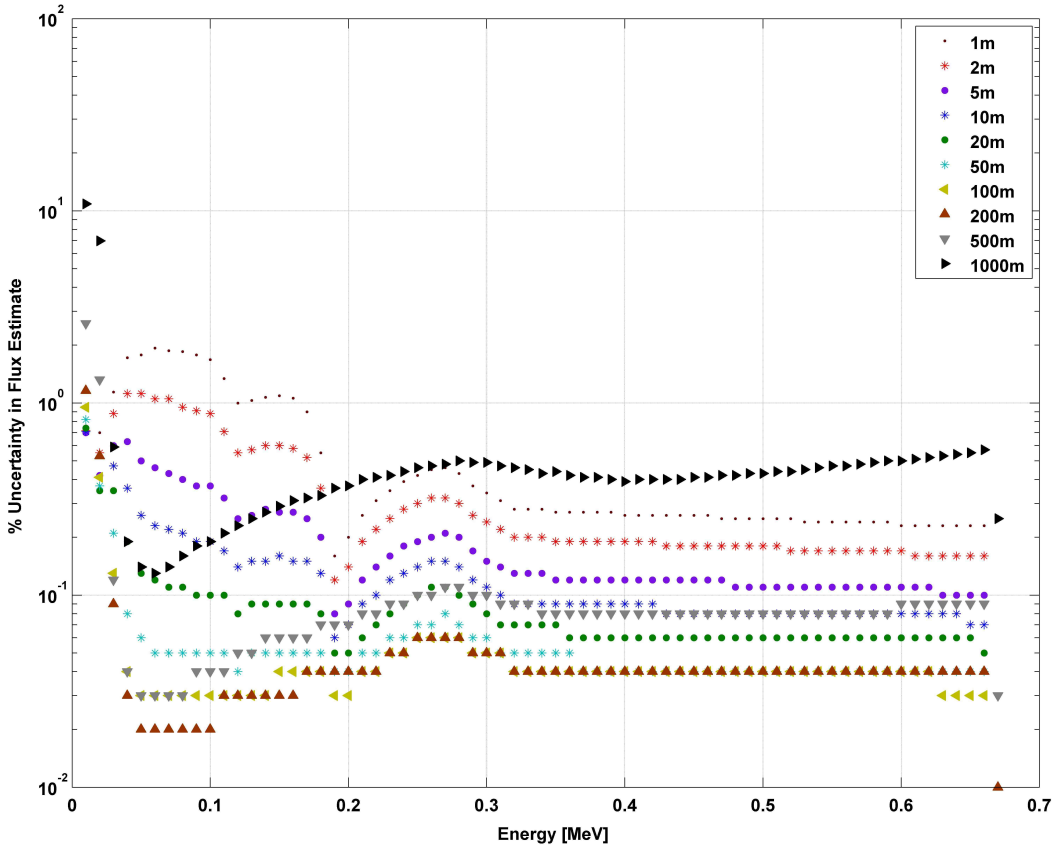

Figure A.2: Percent uncertainty in the MCNP-generated flux estimations as a function of energy (Cs-137 photons in air).

Appendix B | Principles of the Monte Carlo Approximation of Integrals

This appendix outlines the well established foundations of the Monte Carlo approach to approximating the integration of complex functions [28], [47]–[49]. Not intended as a complete guide to Monte Carlo techniques, the focus here is on the processes, key criteria for implementation, and the principles applied in the development of the BASBP.

B.1 Foundation of Monte Carlo Approximations

As with most statistical endeavors, one most often seeks to characterize a random process by some quantifiable measure(s) or parameters of interest. As examples, the the expected value or mean value (also known as the first moment) and variance are the two most common measures cited to describe a statistical distribution or parameter of interest. The description of Monte Carlo methods for approximating complex integrations begins with the case in which the underlying probability distribution is a function of a single variable. As given by Equation B.2, the deterministic methods for calculating the mean and variance of a function, $f(X)$, with a probability density, $\pi(X)$ are:

$$I(f(X)) = E_X[f(X)] = \int f(X)\pi(X)\mathrm{d}X \tag{B.1a}$$

$$R_{II} = E\left[(f(X) - E[I(f(X))])^2\right] \tag{B.1b}$$

However, where analytical integration fails, the Monte Carlo approximation begins with importance sampling by drawing N independent and identically distributed (i.i.d.) samples, $\{X_i\}_{i=1}^{N}$, from the target distribution, $\pi(X)$. The empirical estimate of the target distribution

is given by:

$$\pi(X) \approx \hat{\pi}_N(X) = \frac{1}{N}\sum_{i=1}^{N}\delta(X - X_i) \tag{B.2}$$

where the subscript N denotes the Monte Carlo approximation. Substituting the empirical distribution, $\hat{\pi}_N(X)$, for the target distribution, $\pi(X)$, in Equation B.1a, the Monte Carlo approximation, $I_N(f(X))$ of the first moment is given by:

$$I_N(f(X)) = \frac{1}{N}\int\sum_{i=1}^{N}(f(X) - \delta(X - X_i)\mathrm{d}X = \frac{1}{N}\sum_{i=1}^{N}f(X_i) \xrightarrow[N\to\infty]{a.s} I(f(X)) \tag{B.3}$$

where the diraq delta function serves as a filtering function for $f(X)$. Similarly, for the variance of the Monte Carlo estimate, $R_{I_N I_N}$, we have:

$$\begin{aligned} R_{I_N I_N} &= \frac{1}{N}\int\sum_{i=1}^{N}[f(X) - I_N(f(X))]^2\delta(X - X_i)\mathrm{d}X \\ &= \frac{1}{N}\sum_{i=1}^{N}[f(X_i) - I_N(f(X))]^2 \xrightarrow[N\to\infty]{a.s} R_{II} \end{aligned} \tag{B.4}$$

Key properties of the Monte Carlo estimate, $I_N(f(X))$, include:

- $I_N(f(X))$ is an *unbiased* estimator of $I(f(X))$;
- $I_N(f(X))$ converges (almost surely) to $I(f(X))$ by the strong Law of Large Numbers;
- The variance of $I_N(f(X))$ is bounded ($R_{I_N I_N} < \infty$);
- Unlike deterministic methods, MC sampling focuses the estimate on the high probability regions of $f(X)$.

B.2 Importance Sampling Methods

Monte Carlo estimation methods all rely on some form of sampling process by which random samples are drawn from the target distribution. While the mechanics of the basic method as described in Section B.1 is straight forward, difficulties can arise when attempting to

sample the target distribution directly. The method of importance sampling overcomes the problems associated with directly sampling by approximating the target distribution, $f(x)$, with a sampling distribution, $q(x)$. Ideally, $q(x)$ approximates $f(x)$ as closely as possible. At a minimum, the support of $q(x)$ must be greater than or equal to the support of $f(x)$. That is, the samples drawn from q must at least cover the region corresponding to samples drawn from f. To approximate the integral of $f(x)$, we integrate the ratio of the target distribution to the sampling distribution, multiplied by the sampling distribution, as given in Equation B.5:

$$I = \int_X f(x)\mathrm{d}x = \int_X \frac{f(x)}{q(x)} q(x)\mathrm{d}x \tag{B.5}$$

Use of a sampling distribution also requires that $q(x)$ possesses the following additional properties [47]:

- $q(x) \geq 0$ for all $x \in \mathbb{R}$; and,
- $\int_{-\infty}^{\infty} q(x)\mathrm{d}x = 1$.

With these characteristics in mind, the following processes outline the use of importance sampling to estimate statistical measures of a posterior distribution (as used in the BASBP). The estimate of the posterior mean (using importance sampling) is given by:

$$\hat{f}_t := E[f(X_t)] = \int_X f(X_t) \left[\frac{\pi(X_t|Y_t)}{q(X_t|Y_t)}\right] q(X_t|Y_t)\mathrm{d}X_t \tag{B.6}$$

Applying Bayes rule to the posterior distribution, the weight function, w_t, is defined as the ratio between the posterior distribution and the sampling distribution:

$$w_t = \frac{\pi(X_t|Y_t)}{q(X_t|Y_t)} = \frac{\pi(Y_t|X_t) \cdot \pi(X_t)}{\pi(Y_t) \cdot q(X_t|Y_t)} \tag{B.7}$$

To overcome the problem of using Equation B.7 (which requires direct knowledge of the normalizing constant, $\pi(Y_t)$, a proportional weight function according to Equation B.8 can be defined as:

$$w_t \propto \frac{\pi(X_t|Y_t)}{q(X_t|Y_t)} = \frac{\pi(Y_t|X_t) \cdot \pi(X_t)}{q(X_t|Y_t)} \tag{B.8}$$

where the normalizing constant has been omitted. Returning to the estimate of the posterior mean given in Equation B.6,

$$\begin{aligned}\hat{f}_t &= \frac{1}{\pi(Y_t)} \int_X f(X_t) \left[\frac{\pi(X_t|Y_t)}{q(X_t|Y_t)}\right] q(X_t|Y_t) \mathrm{d}X_t \\ &= \frac{1}{\pi(Y_t)} \int_X w_t f(X_t) q(X_t|Y_t) \mathrm{d}X_t\end{aligned} \tag{B.9}$$

Using the definition of w_t from Equation B.8,

$$\begin{aligned}\hat{f}_t &= \frac{E_q[w_t f(X_t)]}{\pi(Y_t)} = \frac{E_q[w_t f(X_t)]}{\int w_t \cdot q(X_t|Y_t) \mathrm{d}X} \\ &= \frac{E_q[w_t f(X_t)]}{E_q[w_t]}\end{aligned} \tag{B.10}$$

Returning to the concept of Monte Carlo approximations of integrals, assume that N particles are drawn from the sampling distribution, $q(X_t|Y_t)$, as in Equation B.2:

$$\hat{q}(X_t|Y_t) \approx \frac{1}{N} \sum_{i=1}^{N} \delta(X_t - X_t^i) \tag{B.11}$$

Applying the normalized form of the weighting function, w_t, to Equation B.10, the estimate of the conditional mean of $f(X_t)$ is given by:

$$\begin{aligned}\hat{f}_t &= \frac{E_q[w_t f(X_t)]}{E_q[w_t]} \\ &\approx \frac{\frac{1}{N} \int_X \sum_{i=1}^{N} w_t f(X_t) \delta(X_t - X_t^i) \mathrm{d}X}{\frac{1}{N} \int_X \sum_{i=1}^{N} w_t \delta(X_t - X_t^i) \mathrm{d}X} \\ &\approx \sum_{i=1}^{N} w_t^i f(X_t^i)\end{aligned} \tag{B.12}$$

Similarly, the optimal estimate of the posterior distribution using importance sampling is given by Equation B.13

$$\hat{\pi}(X_t|Y_t) \approx \sum_{i=1}^{N} w_t^i \delta(X_t - X_t^i). \tag{B.13}$$

This concludes the general description of Monte Carlo methods of approximating complex functions of integrals.

Appendix C | Geo-spatial Data Covering MARS Test Site

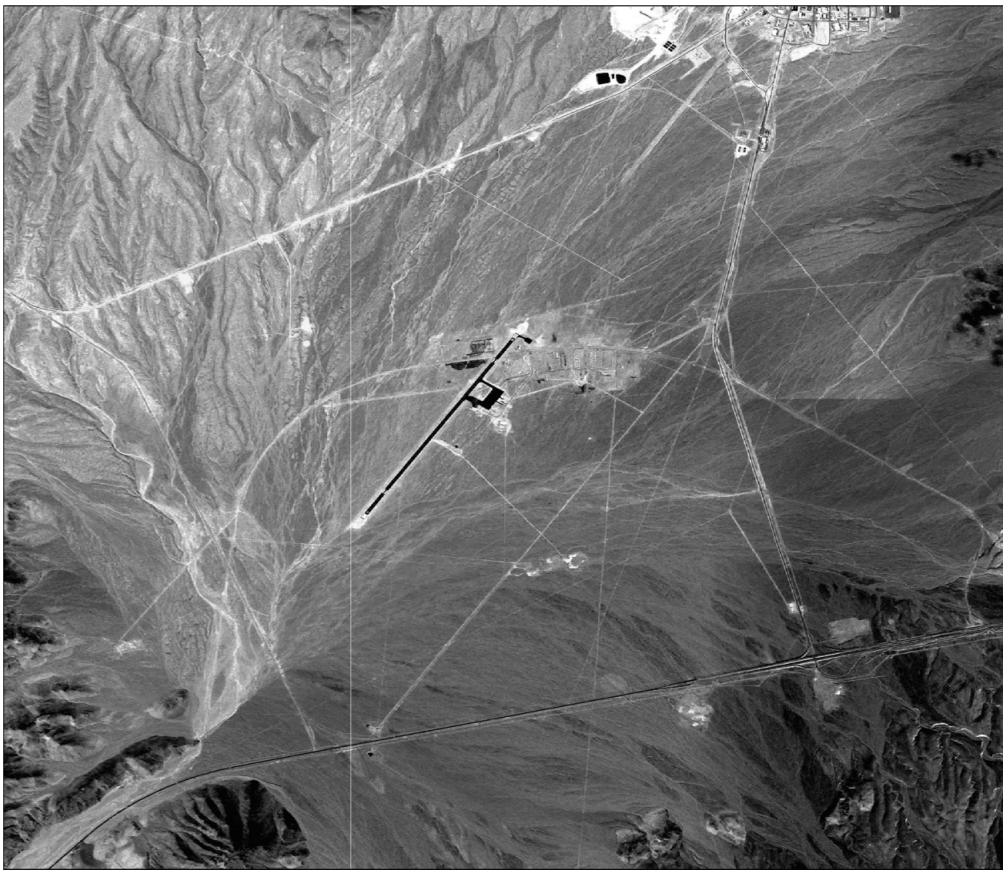

Figure C.1: Satellite imagery of the MARS test site.

(Data obtained from the U.S. Army's Army Geospatial Center digital library [36].)

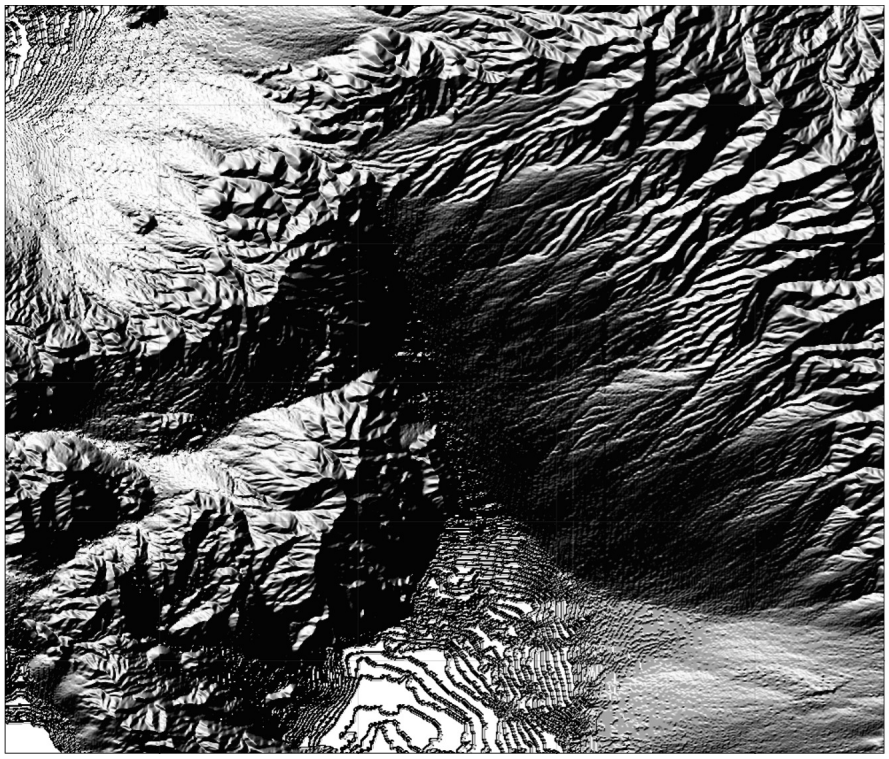

Figure C.2: Depiction of the elevation at the MARS test site.

(Data obtained from the U.S. Army's Army Geospatial Center digital library [36].)

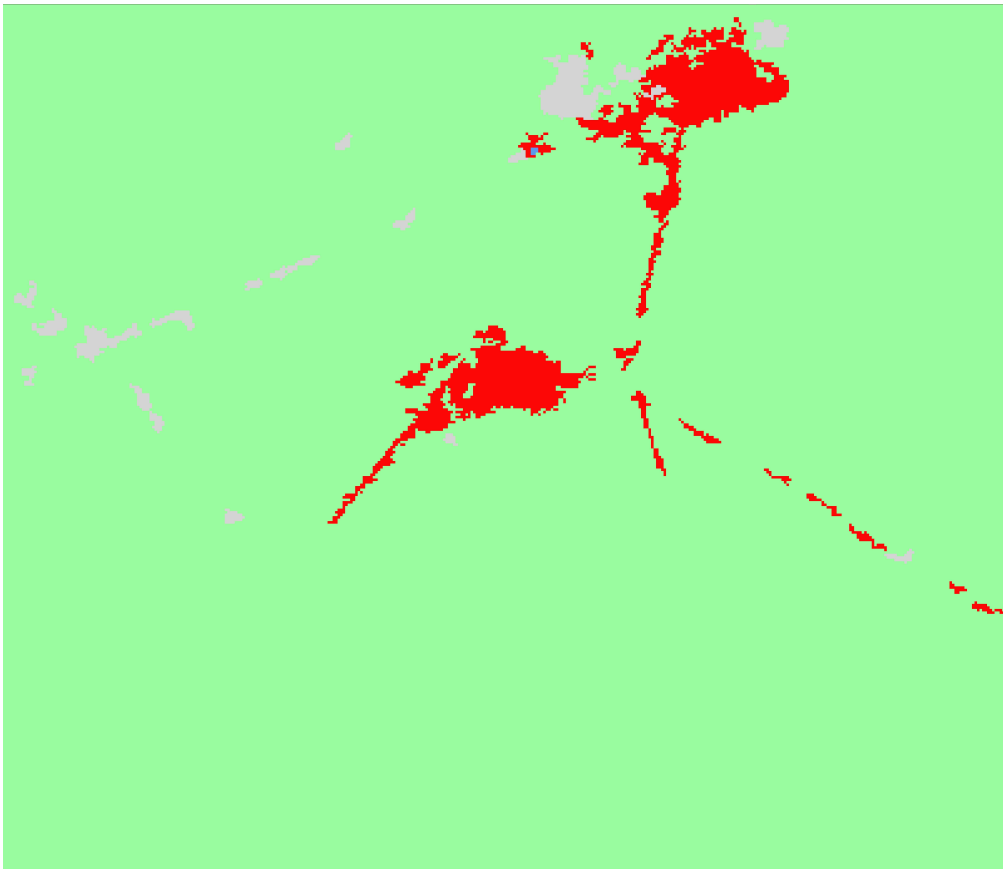

Figure C.3: Depiction of the Geo-Rover land use categories at the MARS test site.

(Data obtained from the U.S. Army's Army Geospatial Center digital library [36].)

Vita

Samuel Willmon graduated from the United States Military Academy at West Point, New York in 1994 with a Bachelor of Science degree in Physics and was commissioned a Second Lieutenant of Infantry. Following graduation, Samuel served in a variety of Infantry assignments in Germany and Korea before being accepted into the graduate program at the Air Force Institute of Technology at Wright-Patterson Air Force Base, Ohio in 2001. After graduating with a Master of Science degree in Nuclear Engineering in 2003, Samuel's became one of the U.S. Army's small number of nuclear and counter-proliferation officers. Samuel has had a variety of assignments, both in the United States as well as while deployed to Iraq and Afghanistan, advising senior commanders and their staff on nuclear and proliferation-related issues. Following graduation from the University of Tennessee, Samuel will continue his active duty service.